

Using a multiscale, probabilistic approach to identify spatial-temporal wetland gradients



Charlotte G. Gabrielsen^{a,b,*}, Melanie A. Murphy^{a,b}, Jeffrey S. Evans^{c,d}

^a Department of Ecosystem Science and Management, University of Wyoming, Laramie, WY 82071, United States

^b Program in Ecology, University of Wyoming, Laramie, WY 82071, United States

^c The Nature Conservancy, Fort Collins, CO 80524, United States

^d Department of Zoology and Physiology, University of Wyoming, Laramie, WY 82071, United States

ARTICLE INFO

Article history:

Received 29 June 2015

Received in revised form 1 July 2016

Accepted 22 July 2016

Available online xxxx

Keywords:

Wetland classification

Random Forests

Nonparametric

Ecosystem services

Gradient

Hydroperiod

Ephemerality

RapidEye

Landsat

ABSTRACT

Wetlands are highly dynamic ecosystem components that fluctuate dramatically in inundation and persistence of water both within and across years. However, these systems are commonly classified in a deterministic, discrete manner that does not reflect inherent spatial and temporal variation. Developing a methodology to identify gradients in water inundation is critical given the dynamic nature of wetlands. We present a methodology that applies probabilistic estimates, derived from a nonparametric model, to predict wetlands along a gradient in ephemerality, or degree of water inundation. We applied this model across four sampling areas in the Plains and Prairie Pothole Region (PPPR) in the U.S. Northern Great Plains. We developed a model relationship between high-resolution (RapidEye) and moderate resolution (Landsat) satellite sensor data. This allowed us leverage the benefits of high spatial resolution data and a long temporal series of freely available mid-resolution data to characterize water persistence in wetlands. To obtain measures of wetland inundation across a gradient of ephemerality, we estimated wetland probabilities across a temporal series reflecting large variation in moisture conditions. We found that a nonparametric statistical approach was highly effective in predicting wetlands of varying size and ephemerality. Our predictions were strongly supported with low error (RapidEye 3.1–15%, Landsat 0.3–1.5%). Probabilistic predictions of wetland ephemerality contribute valuable information needed for management and policy decisions, especially given potential alterations to wetland ephemerality and ecosystem services under climate change. Using predicted gradients in wetland ephemerality over time will enable researchers and land managers to more effectively capture nuance in ecosystem condition, function, and change.

© 2016 Elsevier Inc. All rights reserved.

1. Introduction

1.1. Ecological gradients

A prevalent goal in ecology is to infer how environmental characteristics influence ecological processes, which may represent gradients and not discrete boundaries (Lortie et al., 2004; Manning et al., 2004). Gradients can represent different characteristics of the same process and as such, be expressed in several ways including biotic (e.g., tree height, biomass), abiotic (e.g., soil moisture, soil pH), fractional proportion (e.g., percent of a cover type), or probability of occurrence (McIntyre & Barrett, 1992). Even though gradients are inherent in ecology, traditional remote sensing efforts often classify data into nominal, non-overlapping classes, which notably limits our ability to explore relationships between

environmental and ecological phenomena (Cushman et al., 2010; Evans & Cushman, 2009; Gosz, 1992; McGarigal et al., 2009).

Wetlands are spatially and temporally dynamic, influencing numerous ecological processes in varying magnitudes based on their variation, thus providing an ideal example of landscape features that can be represented as gradients. Wetland ephemerality, or the degree of water inundation, is influenced by complex, interacting factors including wetland type, geology (e.g., wetland substrate and geomorphology), vegetation, climate, weather, and surrounding land uses (Euliss et al., 2004; Jackson, 2006). Gradients may exist within individual wetlands; a single wetland may exhibit a range of ephemerality, from highly ephemeral wetland edges to permanent water storage at a wetland's center. Characterizing gradients of wetland ephemerality captures both their spatial and temporal variability. One way to accomplish this is by predicting the probability of each location being a wetland based on the presence of surface water. Given the importance of diverse wetlands and associated biodiversity for maintaining resilient ecosystems (Folke et al., 2004), documenting the continuum of surface water

* Corresponding author at: Department of Ecosystem Science and Management, University of Wyoming, Laramie, WY 82071, United States.
E-mail address: cgabrie2@uwyo.edu (C.G. Gabrielsen).

inundation, which we will refer to as “wetland ephemerality,” supports a richer understanding of wetlands' functions and contributions to ecosystem health.

1.2. Importance of wetlands

Wetlands play numerous roles in supporting biodiversity, ecological processes, and ecosystem services. These roles include providing breeding and foraging habitat for wetland-dependent species (Gibbs, 2000), enhancing soil moisture and nutrient cycling, influencing soil chemistry, and promoting water filtration, groundwater recharge, flood mitigation, and water storage (Gibbs, 2000; Gleason et al., 2008; Horwitz & Finlayson, 2011). Consequently, biodiversity is proportionally higher adjacent to wetlands (Sabo et al., 2005; Soykan et al., 2012). Additionally, human populations are directly influenced by wetlands' ability to support agriculture, recreation, and pollution reduction (Dale & Connelly, 2012; Horwitz & Finlayson, 2011). All of these wetland services are affected by fluctuations in surface water inundation through time.

Wetland ephemerality is tightly linked to climatic variability and weather extremes, which can cause dramatic temporal fluctuations in wetland water inundation and persistence through time (Johnson et al., 2005; Johnson et al., 2004). Whereas large wetlands can provide persistent water storage and flood mitigation, small, ephemeral wetlands distribute water across the landscape (van der Kamp & Hayashi, 1998), enhance nutrient cycling (Bohlen et al., 1989), and promote landscape connectivity (Compton et al., 2007), making them essential to the maintenance of landscape-level biodiversity.

Wetlands with higher ephemerality tend to be more dependent on precipitation than groundwater (Johnson et al., 2005; Sorenson et al., 1998; Winter & Rosenberry, 1998) and exhibit very high spatial-temporal variation (van der Valk, 2005), making them among the most difficult ecosystem components to classify (Cowardin, 1982; Gallant, 2015; Scott & Jones, 1995). Therefore, wetland classifications capable of capturing spatial-temporal dynamics are an important contribution to wetland monitoring, particularly in assessing ecological impacts of climate change (Ballard et al., 2014; Johnson et al., 2010; Werner et al., 2013).

1.3. Predicting wetland occurrence and spatial-temporal dynamics

Frequent wetland mapping with clear, repeatable methodology is important for monitoring changes in wetland water extent and persistence over time (Töyrä & Pietroniro, 2005). Establishing a record of wetland conditions under current climate provides a baseline from which to compare the presence and persistence of wetland surface water under increased future climate variability. Employing methodology that also estimates gradients of wetland ephemerality is critical given the dynamic nature of these important landscape features. However, there are many challenges associated with mapping wetlands given the extensive complexity of wetland types and wetland dynamics within highly variable landscapes (Gallant, 2015; Ozesmi & Bauer, 2002).

Historical wetland mapping efforts, including those by the U.S. Fish and Wildlife Service National Wetland Inventory (NWI; Wilen & Bates, 1995), were based on aerial photograph interpretation. Although these methods provide highly detailed wetland maps with hierarchical wetland classifications (Cowardin et al., 1979; Cowardin & Golet, 1995), they are often time-consuming and expensive to produce (Finlayson & van der Valk, 1995; Ozesmi & Bauer, 2002). The introduction of satellite remote sensing techniques has improved the accuracy and cost-effectiveness of wetland mapping efforts (e.g., Baker et al., 2006; Ozesmi & Bauer, 2002; Wright & Gallant, 2007). However, a single temporal snapshot of categorically-defined wetland units cannot be used to quantify wetland dynamics. If wetland dynamics and changes in inundation are not monitored frequently, potentially vulnerable wetland complexes (e.g., those with high spatial-temporal variability) may be excluded from management and conservation planning.

Monitoring spatial-temporal variability is a major research need in remote sensing of wetlands (Conly & van der Kamp, 2001). Previous research efforts have demonstrated the utility of such information using multiple approaches (Beeri & Phillips, 2007; Kahara et al., 2009; Niemuth et al., 2010; Wright, 2010). Liu and Schwartz (2012) modeled broad-scale water body densities under a range of varied climatic conditions, providing a spatially explicit portrait of changes in the number and distribution of wetlands of varied size over time. Similarly, Pavri & Aber (2004) monitored wetland change over a period of 15 years, using spectral signatures to map land cover variability (Pavri & Aber, 2004), and Gómez-Rodríguez et al. (2010) employed a time series to monitor spatio-temporal changes of small, temporary ponds (Gómez-Rodríguez et al., 2010). Alternatively, other approaches have characterized changes to wetland size, area, and configuration over time in contrast to fixed NWI-delineated wetland polygons (e.g., Kahara et al., 2009; Niemuth et al., 2010). At a finer spatial scale, other studies have classified levels of wetland inundation along a hydroperiod gradient using surface water and soil moisture data derived from synthetic aperture radar (SAR; e.g., Bourgeau-Chavez et al., 2009; Evans et al., 2014; Gondwe et al., 2010; Lang et al., 2008). Wright and Gallant (2007) performed probabilistic wetland classifications using ancillary environmental data such as soils, slope, and vegetation as a means to predict palustrine wetland types. Likewise, Knight et al. (2013) employed ancillary data and multi-temporal remotely sensed data in a decision tree classification framework; they found that using multiple, varied data types greatly improved wetland mapping accuracy (Knight et al., 2013).

Researchers have also employed a multi-temporal approach to link persistence of water in wetlands to habitat functionality. For example, Rover et al. (2011) analyzed persistence of water in wetland catchments over time to distinguish functional hydrologic wetland classes in the Prairie Pothole Region (Rover et al., 2011), and Pickens & King (2014) found that multi-temporal habitat characteristics best explained marsh bird distributions (Pickens & King, 2014).

Although all these efforts are commendable and valuable contributions, methods that incorporate gradients in wetland ephemerality in both space and time have received little attention (Rover et al., 2011). Gradient analysis approaches can capture spatial variability across landscapes (wetlands representing a continuum of ephemerality), within wetlands (highly ephemeral vs. permanently wet), and through time.

1.4. Objectives

Our objective was to characterize gradients of wetland ephemerality throughout space and time by: (1) modeling fine-scale probability of wetland inundation using high-resolution data (RapidEye); and (2) building a statistical subsampling relationship between high-resolution and moderate-resolution (Landsat) spectral data to model probability of wetland inundation across a longer temporal series. Although the wetland gradient can be wholly represented using RapidEye data, these data have limited historical archives. Therefore, we employed the RapidEye to Landsat spectral subsampling relationship to leverage Landsat's long temporal data archives and estimate the probability of wetland inundation for a given data acquisition time point. By developing a method to identify gradients in wetland ephemerality, we aimed to depict the ecological complexity of wetlands across space and time.

2. Methods

2.1. Study area

Our study area was the Plains and Prairie Pothole Region (PPPR) of the Northern Great Plains of the United States. The PPPR spans roughly 800,000 km² encompassing Montana, North Dakota, South Dakota, as well as parts of Wyoming, Minnesota, and Iowa (Fig. 1; Plains and Prairie Potholes Landscape Conservation Cooperative). The PPPR is an

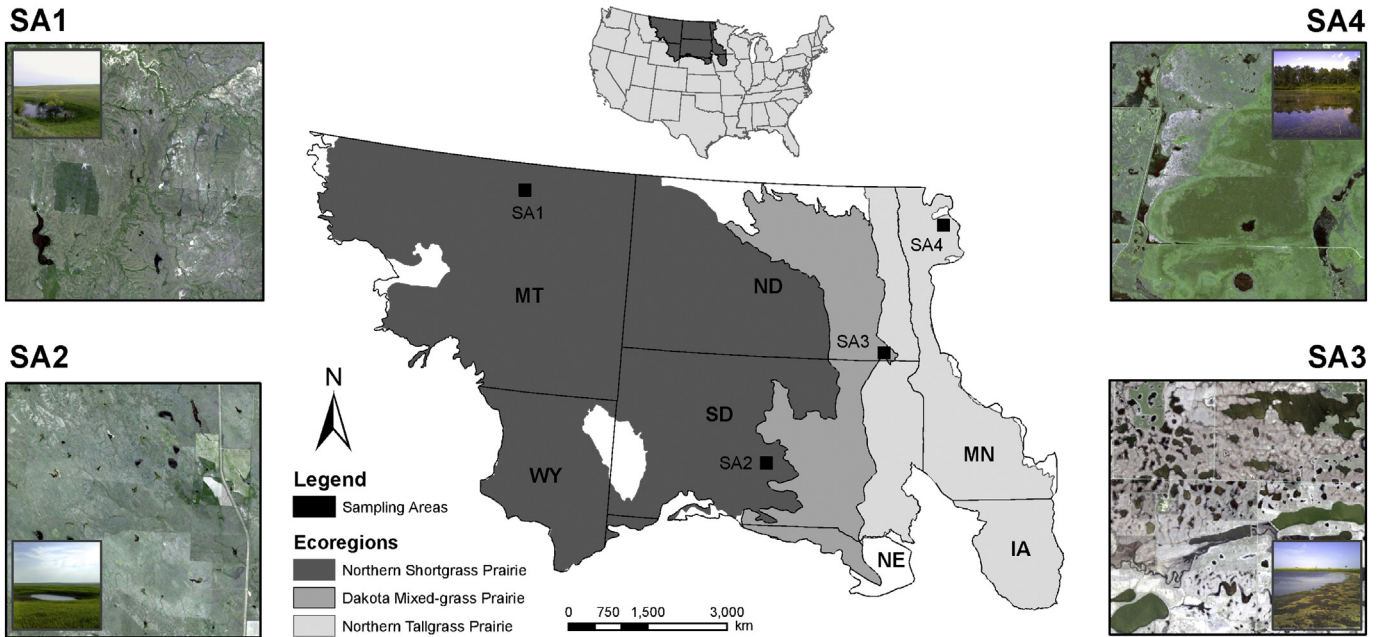


Fig. 1. Map of the four sampling areas across the Plains and Prairie Pothole Region, USA. The shades indicate three ecoregions. Sampling areas are represented by the black squares. Sampling area 1 (SA1) is located in Glasgow, Montana; Sampling Area 2 (SA2) is in Pierre, South Dakota within the Fort Pierre National Grasslands; Sampling Area 3 (SA3) is in Cayuga, North Dakota within Tewaukon National Wildlife Refuge; and Sampling Area 4 (SA4) is within Agassiz National Wildlife Refuge in Middle River, Minnesota. National Agricultural Imagery Program aerial orthoimages and ground photograph insets typify the dominant wetland landscape and wetland type within each sampling area.

ideal location to characterize wetland ephemerality given the region's unique climate and ecology, as well as its high diversity of wetland classes that comprise the extensive wetland network (Euliss et al., 2004; Johnson et al., 2005; Winter & Rosenberry, 1995). Thousands of depressional wetlands formed from glaciation events (*i.e.*, prairie potholes) exist in the PPPR (Euliss et al., 1999), ranging from wet meadows and shallow-water ponds to saline lakes, marshes, and fens (Cowardin et al., 1979). Wetlands in this region receive the majority of their water from snowmelt and rain (Winter & Rosenberry, 1998) and form extensive networks that are hydrologically connected by surface and/or ground water (Winter & Rosenberry, 1995). The degree of connectivity between wetlands, however, varies with time and weather conditions, as well as with the wetlands' position in the landscape (*e.g.*, elevation, soil substrate, topography, proximity to streams or rivers). Regional climate in the PPPR follows a strong north-to-south temperature gradient and west-to-east precipitation gradient (Johnson et al., 2005), creating three distinct ecoregions within the PPPR (Fig. 1; Olson et al., 2001).

We selected four 500 km² sampling areas for our wetland predictions from across all three ecoregions (Northern Shortgrass Prairie, Dakota Mixed-grass Prairie, Northern Tallgrass Prairie), with two sampling areas in the largest ecoregion (Northern Shortgrass Prairie). Although the majority of surveyed wetlands were located on public lands due to access constraints, sampling areas were characterized by a range of land uses, from grazed allotments to leased agricultural fields. Sampling areas were located near Glasgow, Montana on Bureau of Land Management lands (SA1); Pierre, South Dakota, within the Fort Pierre National Grasslands (SA2); Cayuga, North Dakota within Tewaukon National Wildlife Refuge (SA3); and Agassiz National Wildlife Refuge in Middle River, Minnesota (SA4).

2.2. Collection of wetland location data

Within each selected sampling area, we surveyed a minimum of 20 wetlands ($n = 20\text{--}45$) from 15 May to 10 August 2012 and from 10 May to 25 June 2013. To ensure that we captured the range of variation in the landscape, and to prevent biases in the reference training data towards larger, less ephemeral wetlands, we designed our surveys to

capture a range of wetlands of widely varied size (≤ 0.05 ha to ≥ 1600 ha) and ephemerality (highly ephemeral to permanent). We collected wetland location information as point locations where standing water was present using a Trimble Nomad@ 900G GPS (Trimble Navigation Unlimited, Sunnyvale, CA; WGS84 [datum projection], a minimum of 8 satellites, 6.0 Max PDOP, 33.0 Min SNR, minimum of 150 position fixes). Position fixes were differentially corrected using the nearest base station with concurrent data (Trimble Pathfinder Office 5.40; Fig. 2a).

2.3. Spectral data

2.3.1. High-resolution RapidEye data

For the entirety of each of the four sampling areas, we acquired high-resolution (5 m) cloud-free RapidEye scenes (BlackBridge, Berlin, Germany; spectral range 440–850 nm, including a 440–510 nm blue band, 520–590 nm green band, 630–685 nm red band, 690–730 nm red-edge band, and a 760–850 nm near-infrared [NIR] band) at three points in time representing extremely dry (25 June 2012, 22 July 2012, 12 September 2012, 27 September 2012), extremely wet (3 May 2011, 3 June 2011, 8 July 2011, 30 July 2011), and moderate moisture conditions (26 July 2010, 8 September 2011, 5 May 2013, 10 June 2013), for a total of 12 scenes. All RapidEye data were geometrically aligned and orthorectified using ground control points (GCPs) and fine digital elevation models (DEMs) by the vendor (BlackBridge, Berlin, Germany).

2.3.2. Moderate-resolution Landsat data

We acquired moderate resolution (30 m) Landsat 5 Thematic Mapper (TM) imagery (0.45–2.35 μm spectral range, including band 1 blue visible, 0.45–0.52 μm ; band 2 green visible, 0.52–0.60 μm ; band 3 red visible, 0.63–0.69 μm ; band 4 NIR, 0.76–0.90 μm ; band 5 NIR, 1.55–1.75 μm ; band 7 mid-infrared, 2.08–2.35 μm) with $\leq 10\%$ cloud cover through the USGS Earth Explorer interface (<http://earthexplorer.usgs.gov>). For each sampling area, we acquired Landsat imagery for six years, at three points in time across the growing season: early (May 5–May 30), mid (July 5–July 30) and late (August 4–Sept 30) season, with the years representing variation in precipitation (two “dry”

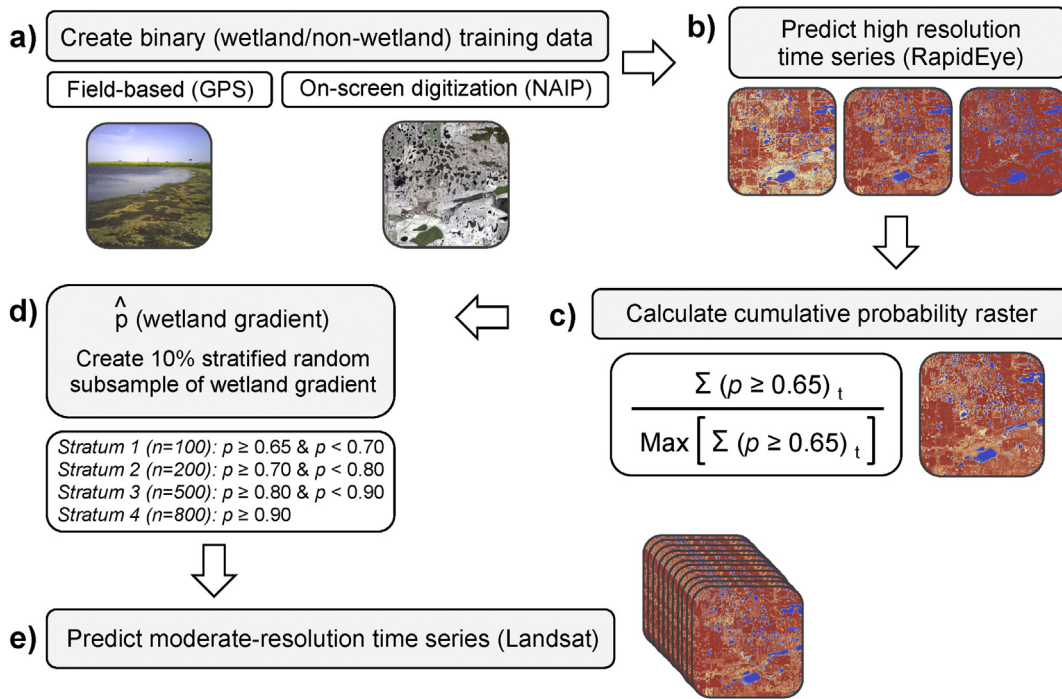


Fig. 2. Workflow diagram of the probabilistic and multiscale modeling framework for the wetland probability classifications. NAIP = National Agriculture Imagery Program.

years [1988, 2002], two years of “moderate” precipitation [1984, 1999], and two “wet” years [1993, 2011]), for a total of 18 scenes (Table 1). We selected these years using NOAA data of average yearly precipitation in the Northern Rockies and Plains climate region (West North Central States) of the United States over the past 30 years (NOAA, 2013). Across the 30-year time-span, “dry” years represented the minimum ($366 \leq 386$ mm) average precipitation/year; “moderate” the median ($467 \leq 480$ mm) average precipitation/year; and “wet” the maximum ($549 \leq 605$ mm) average precipitation/year.

We used dark-object subtraction (Chavez, 1996; Chavez, 1988) to atmospherically correct all Landsat spectral data (bands 1–5, and 7) to at-satellite reflectance values (Song et al., 2001). To represent characteristics associated with both upland and wetland variation, we calculated the tasseled cap transformation (Huang et al., 2002) and

Modified Soil Adjusted Vegetation Index (MSAVI; Huete, 1988; Qi et al., 1994), resulting in a total of six bands and four spectral components used in the model. The tasseled cap transformation represents brightness, greenness, and wetness attributes (Huang et al., 2002), which are sensitive to soil, vegetation structure, and water. MSAVI provides a vegetation index that compensates for background soil reflectance and vegetation senescence (Qi et al., 1994), both characteristic of semi-arid prairie landscapes. All image processing was performed with user-developed SML scripts in ERDAS Imagine 11.0.4 (Intergraph 2011).

2.4. Prediction of RapidEye wetland gradient

We derived training data for our wetland predictions from a combination of field-based data collection (20–45 wetlands/sampling area, as

Table 1

Descriptions of Landsat data acquisitions for each sampling area across the temporal series. ‘PPT’ represents the average yearly precipitation conditions across the Northern Rockies and Plains climate region. ‘Season’ represents the relative timing of Landsat data acquisitions across the growing season within each of the designated years in the temporal series. Dates indicate the Landsat data acquisition dates corresponding to each condition within each sampling area.

Year	PPT	Season	Sampling areas			
			SA1	SA2	SA3	SA4
1984	Median	Early	1-May-1984	23-May-1984	16-May-1984	14-Apr-1984
		Mid	20-Jul-1984	NA	3-Jul-1984	19-Jul-1984
		Late	21-Aug-1984	27-Aug-1984	5-Sep-1984	NA
1988	Dry	Early	10-Apr-1988	NA	27-May-1988	27-May-1988
		Mid	15-Jul-1988	5-Jul-1988	NA	30-Jul-1988
		Late	1-Sep-1988	22-Aug-1988	15-Aug-1988	NA
1993	Wet	Early	10-May-1993	16-May-1993	25-May-1993	NA
		Mid	29-Jul-1993	NA	NA	NA
		Late	14-Aug-1993	4-Aug-1993	NA	30-Sep-1993
1999	Median	Early	25-Apr-1999	1-May-1999	24-Apr-1999	26-May-1999
		Mid	14-Jul-1999	NA	13-Jul-1999	13-Jul-1999
		Late	16-Sep-1999	6-Sep-1999	14-Aug-1999	NA
2002	Dry	Early	19-May-2002	25-May-2002	18-May-2002	18-May-2002
		Mid	6-Jul-2002	NA	5-Jul-2002	NA
		Late	23-Aug-2002	14-Sep-2002	7-Sep-2002	7-Sep-2002
2011	Wet	Early	15-Jul-2011	NA	NA	25-Apr-2011
		Mid	NA	NA	NA	28-Jun-2011
		Late	16-Aug-2011	7-Sep-2011	NA	16-Sep-2011

‘NA’ indicates time points where images with $\leq 10\%$ cloud cover were unavailable

described in section 2.2 above) and on-screen digitizing of National Agriculture Imagery Program (NAIP) orthoimagery with a minimum of 285 training samples in low-density wetland areas and a maximum of 545 training samples in high-density wetland areas (Fig. 2a). We created a balanced training data set that captured large variability in both the wetland and non-wetland classes. Wetland training data were created from (1) a range of wetlands of widely varied types, sizes, and ephemeralitys, and (2) a range of ephemeralitys from across individual wetlands (i.e., training data were created from both wetland centroids and from vegetated wetland edges). Non-wetland training data were created to capture a range of non-wetland cover types. To minimize potential biases associated with varied moisture conditions over time, we merged training data created independently for each of the three RapidEye scenes to create a consolidated training dataset for wetland predictions within each sampling area. We defined each training observation as wetland [1] or non-wetland [0] to create a binomial dependent variable.

Using the field and digitized training data, we predicted wetland probability for each RapidEye image using Random Forests (RF; Breiman, 2001) in the R package randomForest (Liaw & Wiener, 2002; Fig. 2b). For binary classifications using Random Forests, p is the predicted probability of “success” (in this case, presence of water), where probabilities of 1 (water occurrence) and 0 (non-occurrence) are symmetrical (Cutler et al., 2007; Hastie et al., 2001; Liaw & Wiener, 2002).

As a nonparametric bootstrapped decision tree method, Random Forests: (1) affords strong predictive capacity for binomial models, (2) minimizes bias in sparse feature spaces (Biau, 2012), (3) accounts for parameter interactions (Breiman, 2001), and (4) is capable of handling complex nonlinear relationships. Additionally, the convergence of the plurality in the votes matrix scales to a probability distribution directly comparable to a logistic regression model (Cutler et al., 2007; Hastie et al., 2001; Liaw & Wiener, 2002) and has been used extensively in species distribution modeling (e.g., Cutler et al., 2007). The model was predicted using the R package “raster” (Hijmans et al., 2014) to create a raster representing the probability ($p = 0-1$) of a pixel being inundated with water (Fig. 2b).

For the purpose of estimating model performance, we classified pixels with $p \geq 0.65$ as wetlands (Fig. 2c). As an additional evaluation of model performance, at the class level, we performed sensitivity analyses on a probability threshold $p \geq 0.65$ as wetlands (Fig. 2c), evaluating difference in sensitivity-specificity (Fig. A1) across a range of probability thresholds with 0.05 breaks. With our data, a $p \geq 0.65$ is likely a fairly aggressive probability threshold but is also commonly used for RF classification models (e.g., Breiman 2001). The sensitivity test supports using a $p = 0.65$ threshold as a stable measure of error and performance (Fig. A1) making it useful for validation purposes where a “true” continuous distribution is not available for assessing residual model error.

2.4.1. RapidEye model fit and performance

For all RapidEye RF predictions, we assessed model fit using out-of-bag (OOB) error, an estimate of internal model error (Fig. 3A). We calculated OOB error by conducting 5000 bootstrap replicates with replacement using a 34% data-withhold (Breiman, 2001; Fig. 3A). We tested overall model significance using 1000 permutations (Murphy et al., 2010). We generated p -values for the model significance tests using a non-parametric bootstrap: randomizing the wetland training observations 1000 times, and then building a Random Forests model for each randomization to create a null distribution of OOB error (Murphy et al., 2010). We considered a model to be significant if it was below the first percentile on the OOB error distribution ($p < 0.01$).

We assessed model performance by performing 999 bootstrapped cross-validations of all RapidEye RF models ($n = 12$; Fig. 3B). Each bootstrap ($n = 999$) consisted of a 10% data-withhold through the entire RF model and 5000 RF bootstrap replicates (34% data withhold for each replicate), followed by prediction to the 10%-withheld data from

the entire model (Evans et al., 2011; Murphy et al., 2010). We reported model performance as “model performance percent correctly classified” (PCC_p), the percentage of classifications (overall [wetland, non-wetland]) correctly matching their true status.

Lastly, we evaluated the stability of our models by plotting the predicted wetland probabilities from the final RF model versus the predicted wetland probabilities derived from the 999-fold bootstrapped cross-validations. To do so, we indexed the estimated probabilities associated with each withheld wetland data point in the cross-validation tests of each model. We then fit the test model without the withheld data and predicted the probabilities for the data withhold.

2.4.2. RapidEye model validation

We validated all RapidEye wetland ephemerality models for which temporally concurrent NAIP imagery was available (Fig. 3C): SA1 (2011 [wet], 2013 [moderate]), SA2 (2012 [dry]), and SA3 (2010 [moderate], 2012 [dry]). We created 150 wetland and 150 non-wetland validation points in ArcMap for each NAIP image via on-screen digitization. We intersected these points with the final wetland model predictions as a true independent validation dataset. We reported model validation accuracy as “validation percent correctly classified” (PCC_v; Fig. 3C).

2.5. Wetland domain

For each sampling area, we generated a raster representing the gradient of wetland inundation across years of varied moisture conditions (wetland domain). This was done solely for the purpose of creating a training dataset for predictions of the Landsat images (described below in Section 2.6). To generate the wetland domain raster, we created a cumulative probability raster by summing the probabilities from each of the three classified RapidEye images within each sampling area. We then divided all summed probabilities by the maximum value of the sums across each raster to rescale the cumulative distribution (Fig. 2c; Fig. 4).

2.6. Prediction of Landsat wetland gradient

To capture the spatial gradient of wetland ephemerality, we took a 10% stratified random subsample (strata defined below) of the wetland domain, weighted by the cumulative probability distribution estimates (Fig. 2d). The stratified random sample was drawn from points representing the cell-centers of a 30-meter resolution Landsat scene to prevent multiple sample points from occurring in the same Landsat pixel, which would introduce pseudoreplication (Hurlbert, 1984). We randomly selected a weighted sample of points associated with each stratum to capture the gradient in wetland ephemerality according to the observed distribution of wetland types in each sampling area. As there were more wetlands composed of higher probability pixels than lower probability pixels across the gradient, we assigned a greater number of points for wetland pixels that were classified with higher probabilities, minimizing zero-inflation. The following sample sizes were used for the strata: Stratum 1 ($p \geq 0.65$ and $p < 0.70$) $n = 100$; Stratum 2 ($p \geq 0.70$ and $p < 0.80$) $n = 200$; Stratum 3 ($p \geq 0.80$ and $p < 0.90$) $n = 500$, and Stratum 4 ($p \geq 0.90$) $n = 800$. A complementary sample of 1600 points was created from pixels with $p < 0.65$ to represent the non-wetland class. This gradient sample formed the training data to build the subsampling relationship with the Landsat data.

We predicted wetlands in Landsat images matching the spatial extent of the RapidEye data from three time points per growing season across six specified years (1984, 1988, 1993, 1999, 2002, 2011) using RF models (Fig. 2e). We trained the Landsat models by assigning Landsat spectral data and component values to the stratified random samples generated from the method described above. The model result was a probability raster (0–1), where pixels $p \geq 0.65$ were classified as wetlands for the purpose of model validation.

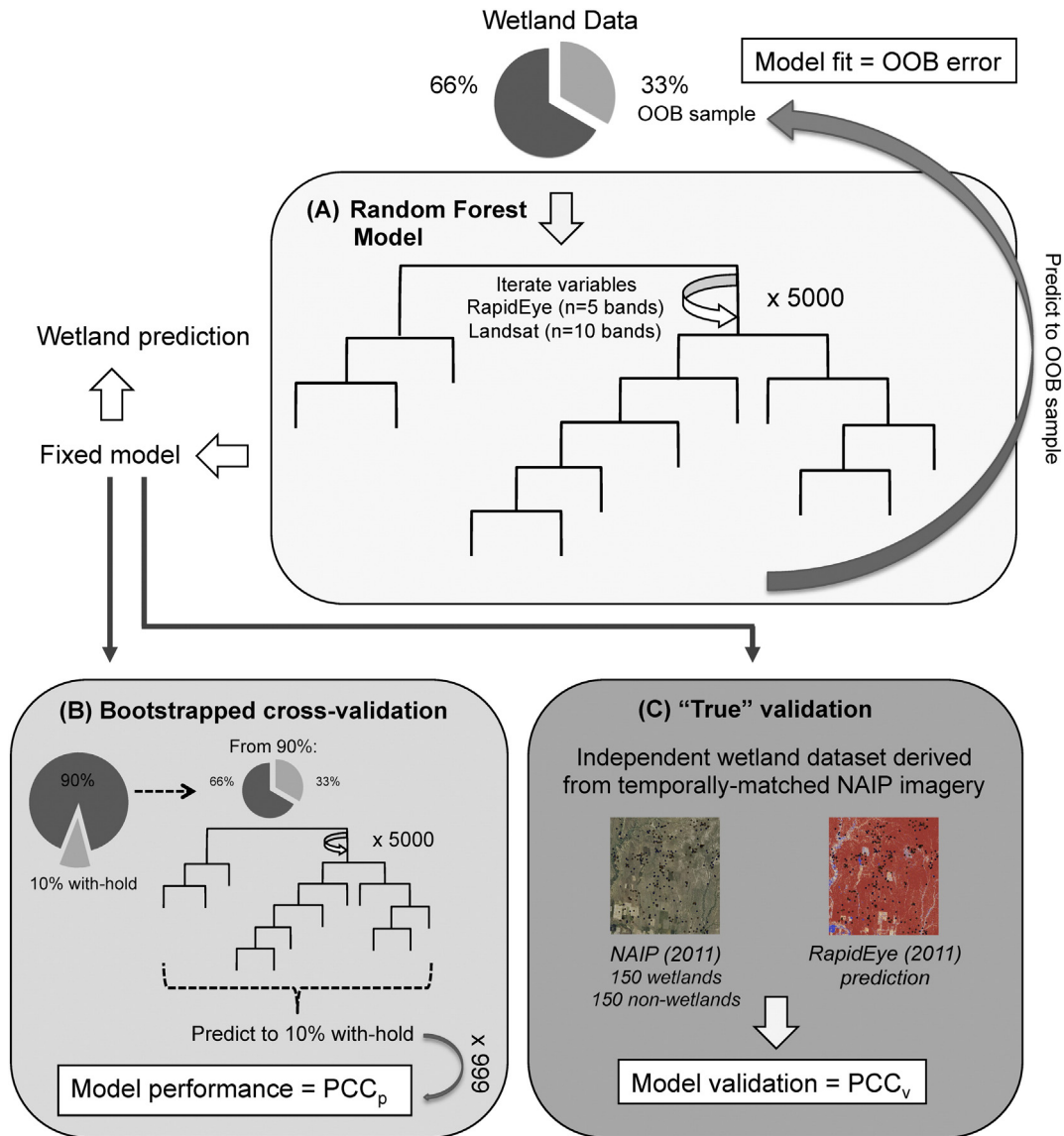


Fig. 3. Derivation of statistics used to evaluate each class of models. For the Random Forest models (A), model fit was assessed using out-of-bag (OOB) error. Model performance for both RapidEye and Landsat was assessed with PCC_p (model performance percent correctly classified) from the bootstrapped cross-validation (B). Validation of the RapidEye predictions (C) was evaluated as “model validation” and reported as PCC_v (validation percent correctly classified).

2.6.1. Landsat model fit and performance

We evaluated model fit and performance of all Landsat RF models using the same methods as for the RapidEye RF models (see Section 2.4.1. and Fig. 3A–B), with the exception of the PCC_v step (Fig. 3C). Due to the fact that (1) freely available high resolution imagery (e.g., NAIP) does not exist for the full temporal span of Landsat images employed and (2) field sampling efforts across the full 30-year temporal series were not realistic, traditional remote sensing validation methods were untenable. Accordingly, model fit and validation statistics for the Landsat RF models did not provide what would be considered a fully independent accuracy assessment, but instead evaluated the ability of the Landsat analyses to replicate the RapidEye data analyses.

2.7. Spectral separability

We used nonmetric multidimensional scaling (NMDS) to: (1) evaluate the ability of RapidEye and Landsat imagery to spectrally discriminate between wetland and non-wetland classes, and (2) identify a gradient of wetland ephemerality. NMDS is a nonparametric multivariate ordination approach that quantifies the degree of dissimilarity

between observations based on a matrix of Euclidean distance (Kruskal, 1964), which can be interpreted as a gradient of membership across a low-dimensional space. As such, NMDS allowed us to visualize the degree of separability between spectra associated with the wetland and non-wetland training data points.

We scaled the spectral values for the RapidEye (5 bands) and Landsat data (6 bands, 4 components) associated with the wetland and non-wetland training data, and plotted three NMDS dimensions for each sensor. In addition to evaluating separability between the two classes, we plotted the results according to predicted probability of inundation, with a color ramp distributed equally into 10 probability classes to demonstrate spectral separability across the ephemerality gradient.

3. Results

3.1. High-resolution (RapidEye) wetland predictions

RF predictions generated from the high-resolution RapidEye data for all four sampling areas across the PPPR (Fig. 5) exhibited high model fit.

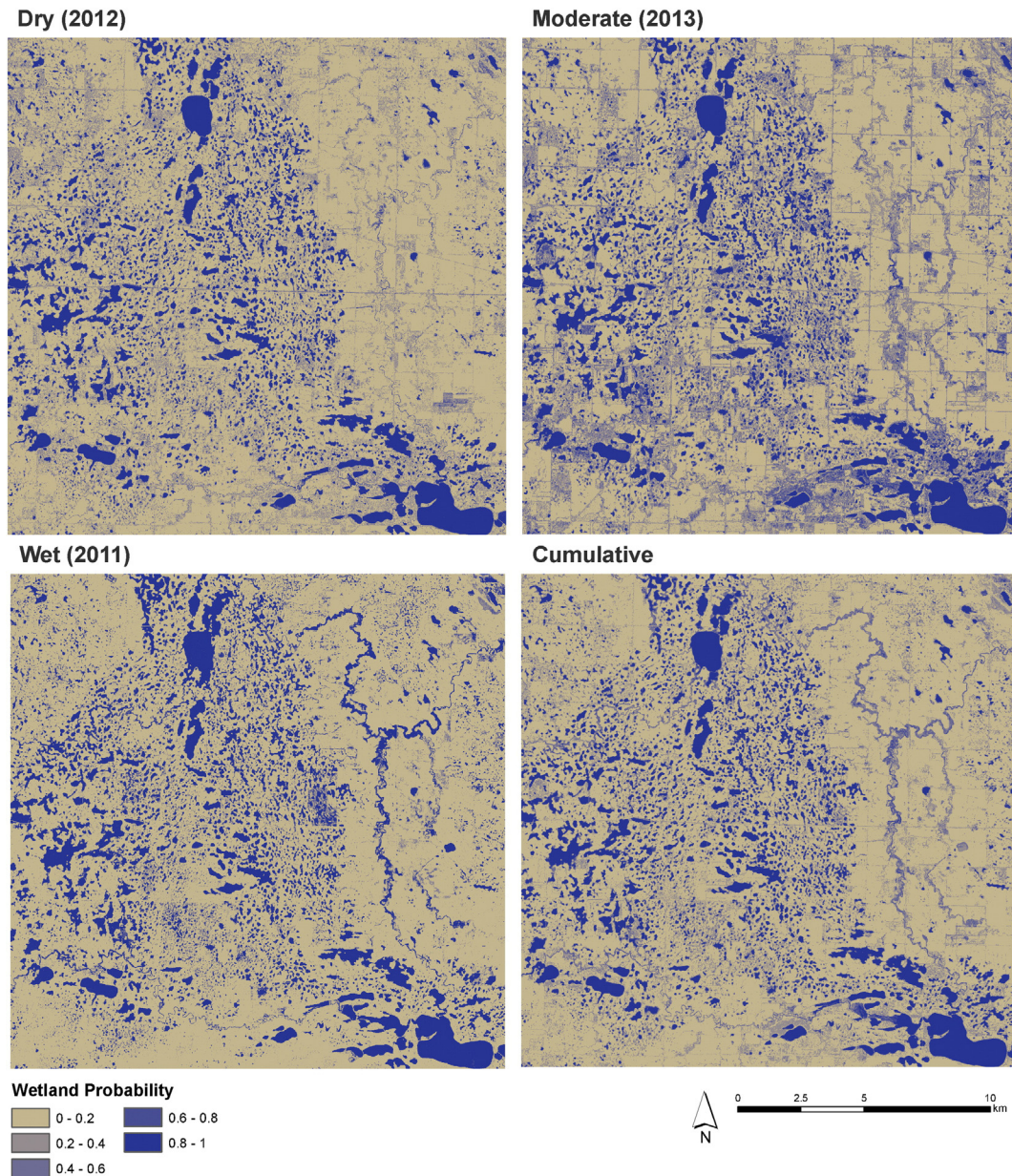


Fig. 4. Examples of RapidEye probabilistic predictions used to generate a raster of cumulative wetland probabilities in SA3. To calculate the cumulative wetland probabilities, estimated wetland probabilities were summed from predictions of RapidEye data collected across three years of varied moisture conditions and divided by the maximum value of the calculated sums. Wetland probabilities were calculated from RapidEye images predicted for a “dry” (2012), “moderate” (2013), and “wet” year (2011).

Across the four sampling areas, overall OOB errors ranged from 3.14 to 15% (Table 2), with a mean OOB error of 6.1%. In all probabilistic predictions, OOB error was higher for the wetland class (4.0–18.0%; mean 8.0%) than for the non-wetland class (1.9–12.0%; mean 4.2%). The bootstrapped cross-validation revealed high model performance for all RapidEye prediction models, with a mean PCC_p of 94% (range = 70.2–100%; see Table A1). Although we observed comparatively lower PCC_p for a few of the RapidEye models, the majority of PCC_p values exceeded 90% (Fig. 6). When models were validated against independently-derived validation data, all PCC_v estimates were >91% (range = 91.0–97.7%; Table 3). All models were highly significant ($p < 0.001$; Table A1) using a non-parametric bootstrap (Evans & Murphy, 2015; Murphy et al., 2010) and stable (Fig. 7).

In general, model fit increased as amount of moisture increased (Table 2). Although OOB error was low overall, the highest OOB error corresponded with classifications at “dry” time points, when overall inundation was at a minimum, in all sampling areas but SA4. Conversely,

low OOB error generally corresponded with image classifications from “wet” time steps (Table 2). The lowest and most uniform OOB error was observed for wetland classifications in SA4 in northeastern Minnesota within the Northern Tallgrass Prairie, with <5% OOB error across all three time steps of varied moisture conditions (Table 2). In contrast, SA2, in central South Dakota within the Northern Shortgrass Prairie, exhibited the highest OOB under both “wet” and “dry” time steps, and the second highest OOB error under “moderate” moisture conditions (after SA3; Table 2).

3.2. Moderate-resolution (Landsat) wetland predictions

When we upscaled RapidEye wetland predictions to moderate-resolution Landsat images from each of the corresponding sampling areas (Fig. 5), we observed high model fit in the resulting probability estimates (OOB error mean = 0.8%; range = 0.3–1.5%; Table 4, Table A2). Similar to predictions using the RapidEye data, mean OOB error from

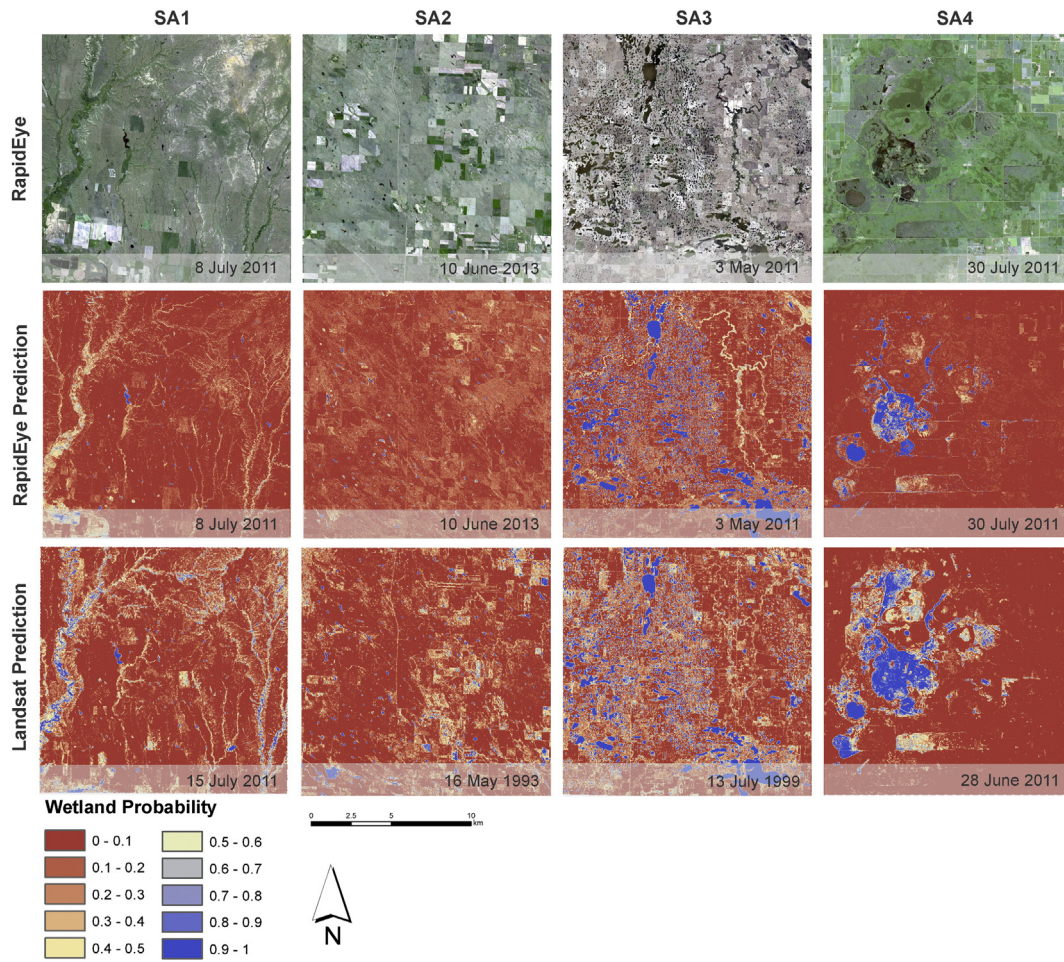


Fig. 5. Examples of probability predictions generated for each of the four sampling areas. For each sampling area, we depict examples of a raw RapidEye image (“RapidEye”), a wetland prediction performed on the RapidEye image (“RapidEye Prediction”), and a wetland prediction performed on Landsat data (“Landsat Prediction”).

the RF Landsat models was higher for the wetland class (mean = 1.8%; range = 0.6–3.2%; Table A2) than for the non-wetland class (mean = 0.02%; range = 0–0.3%; Table A2). Root-mean-square error ranged from 0.06 to 0.12 (Table A2). Overall, OOB error was highly uniform when averaged across years (0.7–1.0%), precipitation conditions (0.83–0.91%), and season (0.73–0.96%), indicating that RF predictions performed comparably across all four sampling areas in the PPPR (Table 4). Furthermore, we observed high model performance for all Landsat model predictions, with a mean PCC_p of 84.7% (range = 65.2–92.5%; Table A2). Some bootstrapped cross-validations (4 out of 52 models) returned relatively low PCC_p (60–70%), but the majority of models performed substantially better, with PCC_p values over 80% (41 out of 52 models; Fig. 6, Table A2). As with the RapidEye models, all models were highly significant ($p < 0.001$) compared to a null distribution (non-parametric bootstrap) and stable (Fig. 7).

Table 2
Out-of-bag (OOB) model error results from Random Forest predictions of RapidEye scenes across three years of varied moisture conditions (dry, moderate, wet) per sampling area. Mean OOB error is calculated across sampling areas under each moisture condition.

Area	Out-of-bag error (%)		
	Dry	Moderate	Wet
SA1	11.21	4.24	3.33
SA2	15.00	5.43	5.98
SA3	8.13	5.90	3.45
SA4	3.14	4.32	3.22
Mean	9.37	4.97	4.00

3.3. Spectral separability

NMDS plots of the RapidEye spectral data in SA1 and SA3 showed distinct clustering of wetland and non-wetland classes (Fig. 8). Though wetlands and non-wetlands classified from Landsat were still relatively clustered, there was overlap of wetlands with the non-wetland spectral space. Wetlands of intermediate probabilities/ephemeralities are intermediate in spectral sign as they share spectral characteristics with both wetlands and non-wetlands. Based on this observation, we argue that our classification of surface water inundation across the landscape as a gradient enables us to capture wetlands across a range of ephemerality. Plots of the wetland probabilities revealed that wetlands in the overlapping spectral region (orange and green points) were of intermediate probabilities spanning the gradient, representing wetlands of intermediate ephemerality (view publication online for color).

4. Discussion

We generated highly accurate predictions of inundation across wetland ephemerality gradients, as well as across a diverse range of landscapes and wetland types in the PPPR. By leveraging fine-scale remotely sensed data (RapidEye), we were able to exploit freely available, moderate-resolution data (Landsat) to assess wetland ephemerality across numerous given time points representing a range of precipitation conditions. By characterizing wetlands as both spatial and temporal gradients *versus* homogenous objects belonging to a single category, our models capture ecological processes and the dynamic nature of wetlands.

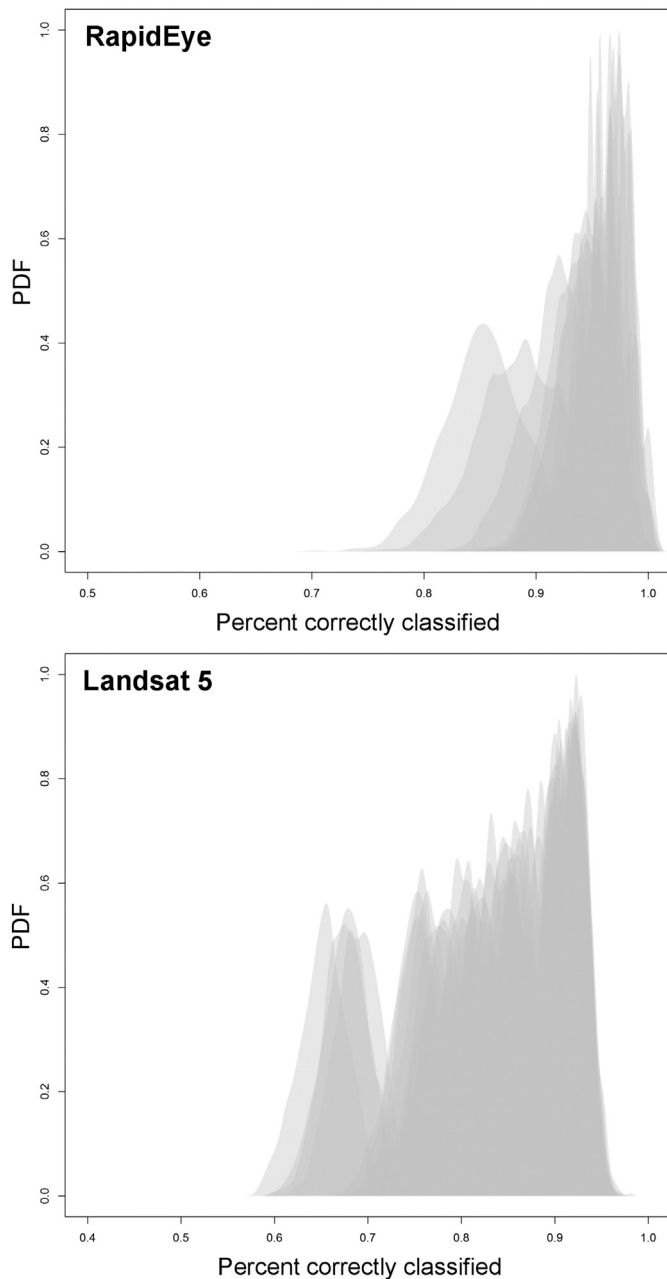


Fig. 6. Probability density function (PDF) plots of model performance percent correctly classified (PCC_p) from all bootstrapped cross-validations of all RapidEye ($n = 12$) and Landsat RF models ($n = 52$). Each PDF curve represents a separate RF model.

The gradients of wetland inundation and ephemerality are extremely flexible and can be classified for project-specific goals (Evans & Cushman, 2009) to support a wide range of research objectives and analytical approaches.

4.1. High model fit across all sampling area predictions

We observed high model fit for predictions of wetlands of varying size (ranging from <0.05 ha to ≥ 1600 ha) and ephemerality across all PPPR ecoregions, regardless of the spatial resolution of the source data (RapidEye or Landsat) or the underlying precipitation conditions at each time point (“dry,” “moderate,” or “wet”). The RapidEye data’s higher dynamic range (associated with bit depth and the addition of the red-edge band) and increased autocovariance (attributed to higher spatial resolution; Ju, Gopal, & Kolaczyk, 2005) resulted in higher variability in model error for RapidEye predictions (OOB = 3.1–15.0%;

Table 3

RapidEye model validation using an independent validation dataset (150 wetlands/150 non-wetlands) derived from NAIP imagery. RapidEye acquisition dates are listed with corresponding NAIP acquisition dates, when available. ‘PPT’ depicts the relative precipitation conditions for each year. ‘PCC_v’ is the validation percent correctly classified (Total % [non-wetland class, wetland class]).

Area	RapidEye	NAIP	‘PPT’	PCC _v (%)
SA1	12 September 2012	NA	–	–
	5 May 2013	23 August 2013	Moderate	93.0 (100, 86.0)
	8 July 2011	21 September 2011	Wet	91.3 (99.3, 83.3)
SA2	27 September 2012	3 October 2012	Dry	91.0 (97.3, 84.7)
	10 June 2013	NA	–	–
	3 June 2011	NA	–	–
SA3	22 July 2012	6 September 2012	Dry	97.0 (97.3, 96.7)
	26 July 2010	3 August 2010	Moderate	97.7 (100, 95.3)
	3 May 2011	NA	–	–
SA4	25 June 2012	NA	–	–
	8 September 2011	NA	–	–
	30 July 2011	NA	–	–

NA indicates that no temporally matched imagery is available.

Table A1) compared to Landsat (OOB = 0.4–1.2%; Table A2). The extremely low OOB error rates associated with the Landsat predictions likely resulted from the smoothing effect that occurred when we upscaled our predictions from RapidEye to Landsat (Vanderbilt et al., 2007).

As expected, we observed higher OOB error in the wetland class compared to the non-wetland class for both RapidEye and Landsat predictions. Given the dramatic fluctuations in surface water inundation within and across years, we expected greater variation in the wetland class. In some years, a pixel classified as a wetland in the training data may not be inundated and would not be classified as a wetland by the RF model. Accordingly, wetland class predictions might exhibit higher model error rates than predictions of the non-wetland class due to the higher variance associated with wetland features through time.

Model fit for the RapidEye RF predictions was highest in the wettest year for all sampling areas but SA4 (Table 2). However, SA4 (Agassiz NWR) had the lowest and most uniform OOB error across years of all the sampling areas (mean = 3.6%, range = 3.1–4.3%; Table 2). The high, uniform model fit provides insight into the spatial-temporal dynamics of wetlands in SA4. Located in the far eastern PPPR, SA4 receives more precipitation than any of the other PPPR sampling areas in this study. Wetlands and shallow, open water cover over 60% of the refuge and are managed through an extensive network of dikes and impoundments (Agassiz National Wildlife Refuge Comprehensive Conservation Plan, 2005). As a result, water levels and inundation remain relatively stable throughout the growing season and across years, leading to less variability in model error rates across the temporal series.

Model fit was lower for sampling areas in drier ecoregions (SA1 and SA2; Table 2), though still high (OOB error = 3.3–15.0%; Table 2). Both of these sampling areas are in the shortgrass prairie, which is generally more arid than the mixed-grass and tallgrass prairies. In the drier sampling areas, wetland densities are relatively low and tend to be located within grazed rangelands. Although many wetlands have been altered to increase water storage, the majority of natural wetlands are highly ephemeral wet meadows or occur along riparian corridors. Linear features, such as riparian drainages, may be more difficult to distinguish from the surrounding upland landscape (Congalton et al., 2002; Johansen et al., 2007) and can cause spectral confusion if the feature widths are less than the image resolution, resulting in the detection of subpixel signals (Congalton et al., 2002). Despite the inherent difficulties in predicting wetlands in drier areas with fewer distinct wetlands, our model still yielded highly accurate predictions using both RapidEye and Landsat data.

4.2. Model performance and stability

We observed the highest model performance in SA4 ($PCC_p = 90.0$ – 92.5% ; Table A2), located in the far northeastern extent of the PPPR. This

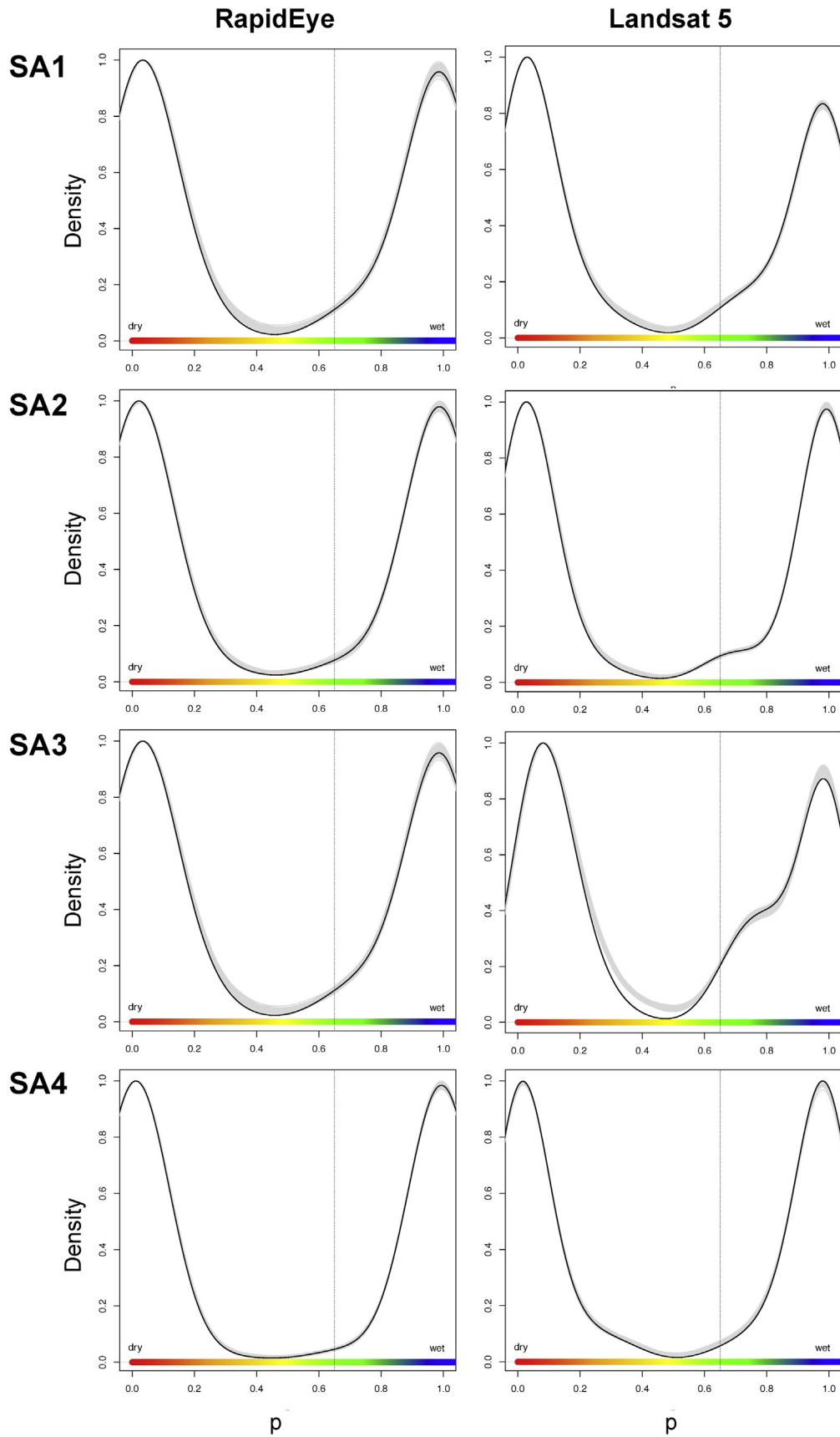


Fig. 7. Probability density function (PDF) plots representing the stability of RapidEye and Landsat 5 models by sampling area. The black curve represents the PDF of the wetland probabilities estimated from the selected RF model; the grey lines represent the model residuals; and the vertical line marks the position of the 0.65 wetland probability threshold. The color ramp on the x-axis corresponds to the colors in the spectral separability plots (Fig. 8), where the red end of the spectrum indicates non-wetland predictions [0] and the spectrum goes to blue as probability of wetland occurrence increases to 1.

result is congruent with the extremely high model fit (lowest OOB error of all four sampling areas) observed for wetland predictions in SA4 (Table A2). Field-based training data for SA4 came from Agassiz NWR, which is located on a glacial lake and encompasses a black-spruce-tamarack bog. The high model performance likely results from the comparatively greater stability in wetland surface water inundation across the sampling area. Accordingly, there is likely less variability in spectral signatures across years.

Model performance (PCC_p) was lowest for models developed to predict wetlands in SA3 ($PCC_p = 65.2\text{--}86.8\%$; Table A2). SA3 contains a high density of inundated wetlands characteristic of the highly glaciated landscape of the Prairie Pothole Region. Here, surface water accumulates in topographic depressions to form depressional wetlands characterized by temporally variable vegetation communities and highly fluctuating surface water extents (Kantrud et al., 1989). As a result, lower model performance is likely due to the high variability in wetland inundation and persistence within and across years.

We observed intermediate degrees of model performance in SA1 ($PCC_p = 75.3\text{--}92.2\%$; Table A2) and SA2 ($PCC_p = 83.1\text{--}92.4\%$; Table A2), both in the shortgrass prairie ecoregion. Here, wetlands are comparatively more difficult to predict, due to the challenges in distinguishing between dry wetlands and the surrounding uplands. We observed a higher proportion of pixels classified with intermediate probabilities of wetland occurrence in these sampling areas. Given our 0.65 wetland classification probability threshold, several training data points representing true wetlands may not have been classified as wetlands by our RF models. This may be especially true in years where wetlands exhibit large fluctuations in inundation. This observation was supported by the results of our independent validation of our RapidEye RF predictions (Table 3; Fig. 3C) with NAIP aerial orthoimagery-derived validation points. We found that PCC_v was considerably higher than PCC_p , indicating that model performance would likely be much higher if we were to validate our models using either wetland observations generated from high-resolution, temporally-matched images, or ground-truthed field survey data.

Overall, models developed for probabilistic predictions of both RapidEye and Landsat data were highly stable, showing strong correlations between the models' wetland probability estimates and the probability estimates resulting from the cross-validation tests on the withheld data (Fig. 7). One observable discrepancy was for the plot of the Landsat models developed for wetland predictions in SA3, in which the models slightly underestimated the wetland probability predictions (Fig. 7). As described above, we believe that lower density of intermediate wetland probabilities from the RF models (observed) compared to the densities from the bootstrapped cross-validations (predicted) in SA3 may be explained by the highly fluctuating nature of wetlands across that sampling area.

4.3. Value of wetland gradient predictions

Despite potential cross-classification errors, identifying areas classified as highly ephemeral wetlands may be informative. Inundated

agricultural fields, such as those prevalent in the eastern PPPR, may share some of the same ecological functions as highly ephemeral wetlands, providing important ecosystem services, such as breeding habitat for amphibians, soil moisture recharge, or waterfowl foraging grounds (e.g. Elphick, 2000). In some cases, flooded agricultural fields may hold water for extended periods of time because they were once wetlands that were tilled and converted to cropland (Wright & Wimberly, 2013).

The impact of spectral confusion on wetland gradient predictions depends on the intended application of our method. If the objective of wetland classification is to identify currently functioning wetlands, then wetland predictions may require *post hoc* correction. One way this could be done is by masking tilled area using available spatial data such as the Cropland Data Layer (CDL) provided by the National Agricultural Statistics Service (Johnson, 2013).

Wetland commission errors in semi-arid regions are a known issue. For example, Baker et al. (2006) found that over-prediction of wetlands corresponded with flood-irrigated fields, which exhibited similar elevation, soils, and spectral signatures as wetlands (Baker et al., 2006). Other potential sources of spectral overlap with vegetated wetlands in this region include shrubs (Daniels, 2006), and wet, bare soils or grassland fire scars (Ozesmi & Bauer, 2002). By using a probabilistic modeling framework, rather than a binary approach, we overcame many of the challenges associated with commission errors, as we observed that features that overlap spectrally were generally classified with much lower probabilities than true wetlands (e.g., irrigated croplands were classified with probabilities ranging from ~0.2–0.4). However, even more prominent commission errors have been found when classifying wetlands in forested landscapes, where areas of dense canopy cover and higher moisture tend to be confused with forested wetlands (e.g., Augusteijn & Warrender, 1998; Li & Chen, 2005; Maxa & Bolstad, 2009). As our study area focuses on grassland systems, further research is needed to test the efficacy of our approach in landscapes with dense forested overstory.

4.4. Use of high-resolution data to leverage moderate-resolution data

We used high-resolution data to train moderate-resolution data, which resulted in a well-fit model that can be applied to predict wetland inundation conditions captured in freely available long-term Landsat data. This mirrors other multiscale research efforts that integrate multiple data types, including LiDAR and optical or visible/infrared data (e.g., SPOT, Landsat; see Geerling et al., 2007; Huang et al., 2014; Hudak et al., 2002; Maxa & Bolstad, 2009), or radar and visible/infrared data (e.g., Augusteijn & Warrender, 1998; Bwangoy et al., 2009; Li & Chen, 2005; Töyrä et al., 2001; Zhu & Tateishi, 2006). These upscaling approaches have been shown to yield more accurate model classifications than imagery solely classified at the higher resolution (De Fries et al., 1998; Hay et al., 2002; Knight et al., 2013; Melendez-Pastor et al., 2010). By using this approach and thresholding the predicted probabilities at 0.65, we were able to identify wetlands across a range of sizes, including small wetlands, which are notoriously difficult to map (Fig. 9; Gallant, 2015; Ozesmi & Bauer, 2002). If we had not used

Table 4
Out-of-bag (OOB) model error (representative of model fit) from Random Forests predictions of Landsat images using a 34% data-withhold at each RF bootstrap iteration (Fig. 3). OOB error was calculated for each sampling area across all six years. OOB error was averaged across years with similar yearly precipitation ('Yearly PPT') and across growing season time periods (early, mid, late). Mean OOB error was calculated across sampling areas for all years, precipitation conditions, and time periods across the growing seasons.

Area	Out-of-bag error (%)											
	Year						Yearly PPT			Season		
	1984	1988	1993	1999	2002	2011	Dry	Median	Wet	Early	Mid	Late
SA1	1.30	1.16	1.10	1.19	0.82	0.73	0.99	1.25	0.91	1.16	0.97	1.03
SA2	0.90	1.10	1.10	0.78	1.13	0.87	1.11	0.84	0.99	1.07	0.73	1.08
SA3	0.54	0.48	0.71	1.01	0.87	0.64	0.68	0.78	0.67	0.81	0.53	0.78
SA4	0.89	0.75	0.96	0.62	0.75	0.55	0.75	0.76	0.76	0.81	0.70	0.76
Mean	0.91	0.87	0.97	0.90	0.89	0.70	0.88	0.91	0.83	0.96	0.73	0.91

high-resolution data, we would likely have missed wetlands smaller than the 30-meter pixel size, thus decreasing model performance. In addition, we were able to make highly accurate (OOB, PCC_p) and consistent (Fig. 7) predictions of probability of wetland inundation to a long temporal series of historical imagery.

4.5. Spectral separability of the wetland gradient

When characterizing wetlands along gradients of ephemerality, the probability distribution itself represents the relative likelihood that a pixel is inundated, given its spectral characteristics (e.g., Cutler et al., 2007; Li & Cutler, 2013). Spectral separability analyses show that model predictions are describing an ecological gradient by discriminating wetlands of varying ephemerality on the basis of their spectral signatures (Fig. 8). The high spectral separability of RapidEye data between wetlands and non-wetlands likely resulted from RapidEye's high spatial resolution, and well as the contribution of the red-edge band (Schuster et al., 2012). The red-edge band is sensitive to differences in plant cover types (Schuster et al., 2012), which may result in greater spectral separability associated with distinctive wetland vegetation.

Spectral overlap between the wetland and non-wetland classes in Landsat (Fig. 8), however, likely resulted from representing the wetland data as a continuous ecological gradient. Instead of classifying the data into two classes (wetland, non-wetland), we predicted a full gradient of wetland occurrence. Intermediate wetland probabilities in the area of spectral overlap represent wetland flux, where wetlands may contain standing water during some time periods and not in others. Furthermore, intermediate wetland probabilities could result from sub-pixel signals, where wetlands may exist but are smaller than the pixel resolution, or from adjacent wetlands with probabilities on extreme ends of the gradient occupying the same pixel. If no gradient existed, the clusters would instead be highly constrained and distinct from each other (Somers et al., 2011).

4.6. Probabilistic predictions

“Classifying” wetland inundation probabilistically enhanced our ability to depict ecological continua, highlighting both wetland change (probability of wetland inundation at time 1 compared to time 2) and inherent wetland stochasticity. Wetland gradients occur not only at the landscape scale, but also within individual wetlands. We observed

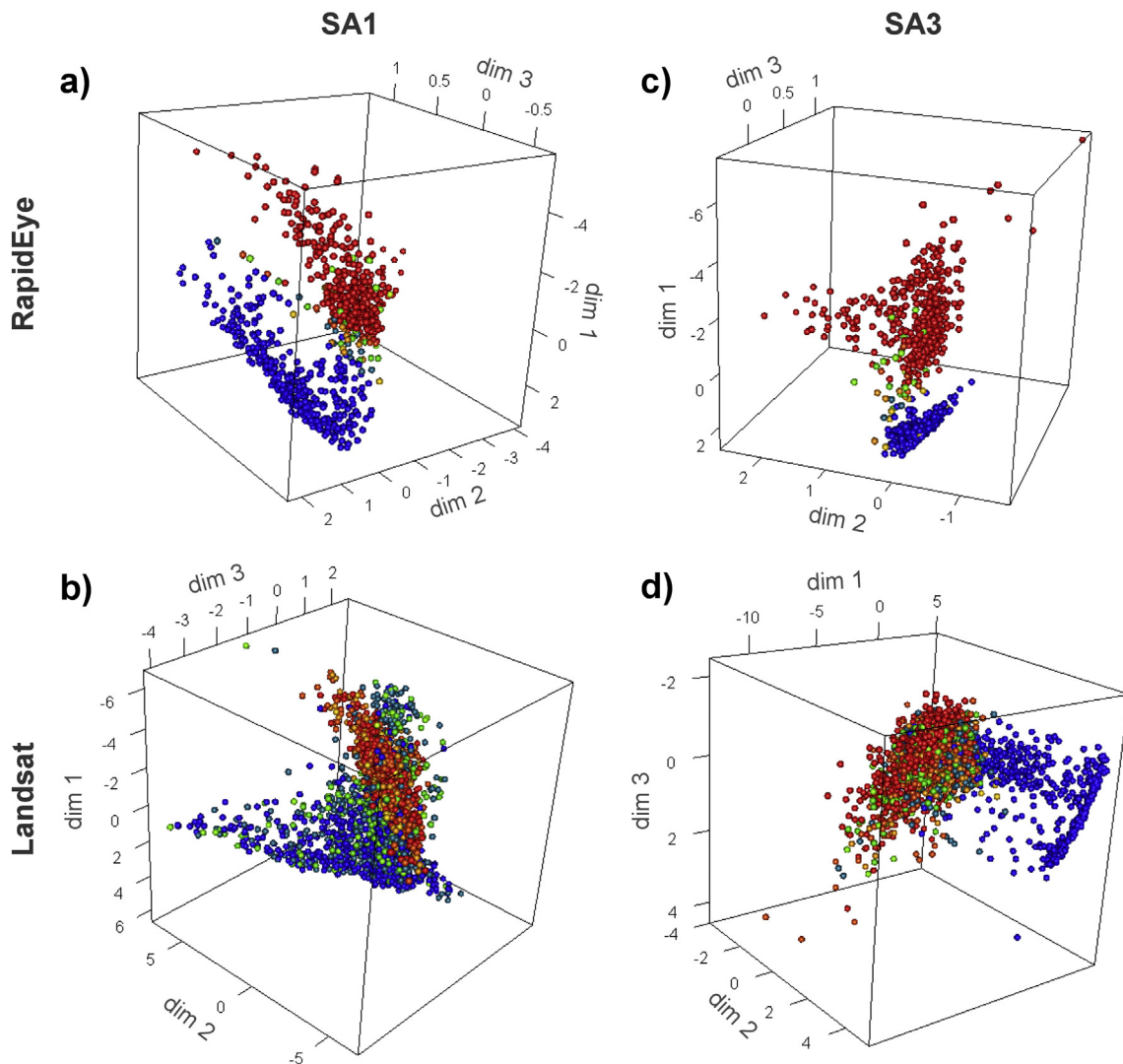


Fig. 8. Three-dimensional visualization of spectral separability analyses performed using nonlinear multidimensional scaling (NMDS). NMDS plots represent spectral separability of wetlands of varying probabilities, and were generated for probabilistic predictions of: (a) RapidEye in SA1; (b) Landsat in SA1; (c) RapidEye in SA3; (d) Landsat in SA3. SA1 (located in an arid region with few wetlands) and SA3 (located in the Prairie Pothole Region, where depression wetlands predominate) represent the two sampling areas that differed most with respect to ecoregion and wetland landscape characteristics. The colors of the points correspond to the color scale in the PDF plots in Fig. 7, where the red end of the spectrum indicates non-wetland predictions [0] and the spectrum goes to blue as probability of inundation increases to 1.

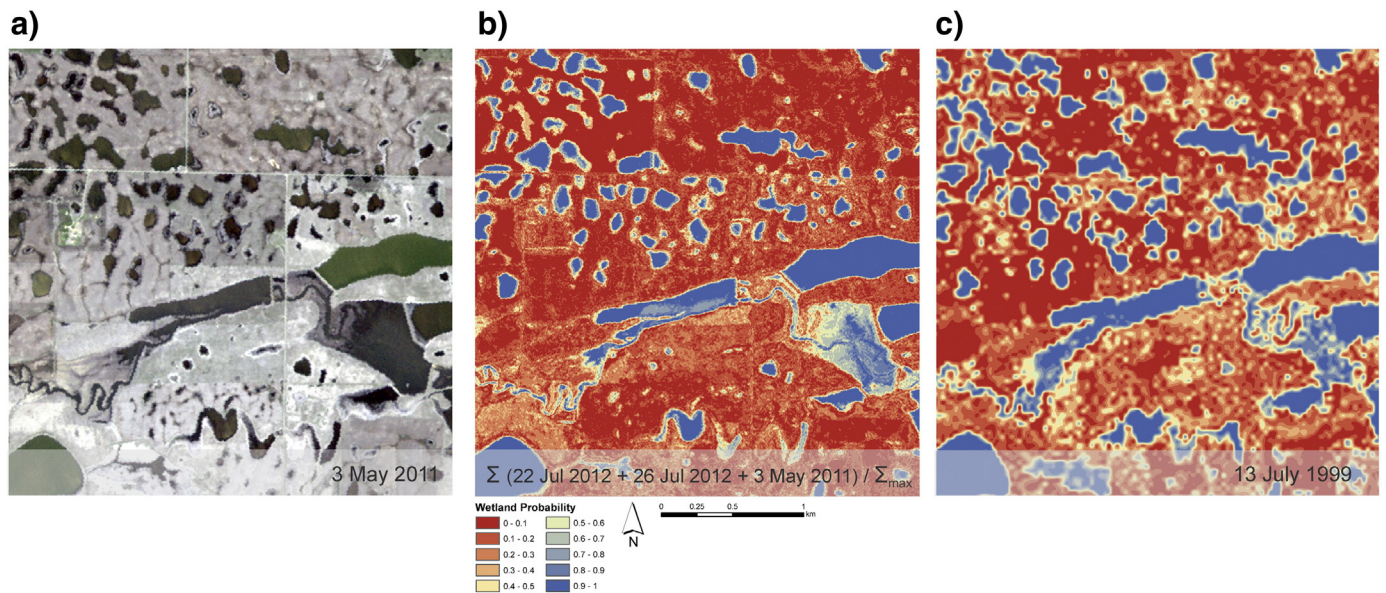


Fig. 9. Multiscale wetland predictions from SA3. From left to right, images represent (a) raw RapidEye image; (b) cumulative probability raster of RapidEye wetland classifications; (c) Landsat wetland classification.

probability gradients around wetland edges in both the RapidEye and Landsat predictions, where the probability of wetland inundation decreased with increasing distance from the wetland's center. This is most likely a function of mixed pixel effects along the wetland edges (Fig. 9). Lastly, since the probability of wetland occurrence is strongly tied to weather conditions (Beeri & Phillips, 2007; Gómez-Rodríguez et al., 2010; Johnson et al., 2004; Kahara et al., 2009), a gradient approach such as ours and other studies that employ a multitemporal approach (e.g., Rover et al., 2011) may improve information for wetland management by identifying wetland areas more susceptible to climatic fluctuations.

4.7. Utility for wetland classification and monitoring

Mapping wetlands over time is critical for conservation, as spatial and temporal changes to wetland networks will affect landscape-wide ecological function. Integrating the wetland prediction techniques developed through this research into planning efforts may provide a more cost-effective and automated method that enables frequent mapping of wetlands over a large spatial extent. The cost of acquiring high-resolution RapidEye data to develop the subsampling relationship with Landsat may be offset by the potential to identify small, highly ephemeral wetlands and ability to utilize a 30+ year data repository. As cloud cover can be problematic during longer-term wet conditions (Zhu & Woodcock, 2012), methods to identify and mask clouds and cloud shadows could be employed to generate model predictions from more time points across the temporal series (e.g., Zhu et al., 2015). Furthermore, if field sampling is infeasible, costs could be further reduced by substituting training data created from temporally-matched high-resolution data, such as NAIP imagery (1 meter spatial resolution). Once training data are developed for an area, the classification framework can be replicated annually. This will allow researchers and managers to investigate spatial dynamics of probability of wetland occurrence through time. With the increased availability of very high-resolution remotely sensed data, accurate wetland classification is more attainable (Gallant, 2015). However, these data are computationally expensive and are available over a shorter temporal series compared to Landsat data. Our method effectively leverages high- and moderate-resolution data to estimate the probability of wetland inundation and the probability that wetlands are wet through time.

Our approach also complements existing wetland classification schemes, which have demonstrated the utility of employing multi-temporal approaches to monitor wetland change and dynamics through time (e.g., Gómez-Rodríguez et al., 2010; Knight et al., 2013; Pavri & Aber, 2004; Rover et al., 2011). We employ a multi-temporal approach that also yields spatio-temporal wetland predictions, but does so as probabilities of wetland inundation, which more effectively represents wetlands as gradients in ephemerality.

4.8. Wetland stochasticity and implications to ecosystem services

Projected changes to temperature, precipitation amount, and precipitation timing may profoundly alter wetland hydrology and wetland ephemerality (Johnson et al., 2005; Ojima & Lockett, 2002). Potential shifts in wetland ephemerality could have major implications for primary productivity, wetland-dependent species complexes, and water availability for human and livestock use. Identifying annual flux in wetlands is a critical indicator of the ecosystem services that they can provide (Carpenter et al., 2006; Zedler & Kercher, 2005). In addition, climate change effects will likely be spatially inhomogeneous (Shaver et al., 2000), making spatially explicit assessments of ephemerality a critical need. By creating spatial predictions of wetland ephemerality under a range of annual weather conditions, we observed “real time” linkages to climatic variation that can be explicitly linked to climate change in the future.

5. Conclusions

We presented a flexible methodology to predict wetland ephemerality gradients using high spatial-resolution data in combination with moderate spatial-resolution data with a longer temporal series. Our intent was to leverage Landsat data, which has been collected at consistent time intervals over a long temporal series, to predict wetland inundation fluctuations over a broad range of climatic (temperature-moisture differences by ecoregion) and inter-annual moisture (weather) conditions. However, our methodology could also be used to monitor rapid changes in wetland dynamics over short time intervals in cases where high temporal-resolution remotely sensed data are available.

Our study employed probabilistic estimates to characterize wetland inundation and ephemerality along a gradient, which reflects ecological

processes and wetland patterns through time more accurately than discrete classifications. Our predictions were highly accurate and our method is amenable to broader-scale, semi-automated wetland monitoring that can provide a cost-effective and detailed complement to existing wetland classification schemes. Predictions of wetland ephemerality are valuable to land managers and scientists given the diverse ecosystem services that wetlands of varying size and ephemerality provide. Moreover, given projected climate change and its implications for water availability within the Plains and Prairie Pothole Region and beyond, it is imperative to better understand the effects of climatic variability upon landscape dynamics and function.

Acknowledgments

Funding was provided by the U.S. Fish and Wildlife Service (USFWS) Plains and Prairie Pothole Landscape Conservation Cooperative,

University of Wyoming Department of Ecosystem Science and Management, EPSCoR Wyoming Center for Environmental Hydrology and Geophysics seed grant, and Wyoming NASA Space Grant Consortium (NASA Grant #NNX10A095H). We thank Greg Knutsen (Agassiz National Wildlife Refuge), Ruben Mares (Fort Pierre National Grasslands), Kristine Askerooth (Tewaukon National Wildlife Refuge), and Randy Dirkson (Montana State Land Board) for their assistance with fieldwork logistics. Lloyd Jones (USFWS) authorized surveys on Waterfowl Production Areas and National Wildlife Refuges in North Dakota and South Dakota. We also thank numerous private landowners for allowing access to their property. We thank field technicians Ellie Stover, Sierra Jech, and Michael Angstadt. Kevin Doherty (USFWS), John Matthews (Conservation International), and Anne Schrag (World Wildlife Fund) provided helpful insight in the early stages of this work. Lastly, we wish to thank three anonymous reviewers for providing valuable feedback on earlier versions of this manuscript.

Appendix A

Table A1

Random Forest model results from prediction of RapidEye images collected across three years per sampling area ('SA'). 'PPT' indicates the relative amount of precipitation for the year classified, and 'n' represents the total number of training points used for the prediction (divided equally into wetland and non-wetland points). For the Random Forests models, the following metrics are reported: Out-of-bag error ('OOB'; representative of model fit) [Total (non-wetland class, wetland class)], producer's accuracy of the wetland class ('Prod.Acc.Mdl' [Overall % (min – max)]), user's accuracy of the wetland class ('Users.Acc.Mdl' [Overall % (min – max)]), and kappa (a measure of model specificity; [mean (diff. between min and max)]). For the bootstrapped cross-validations (n = 1000), percent correctly classified ('PCC_p'; representative of model performance [Mean (min–max)]), producer's accuracy of the wetland class ('Prod.Acc.CV' [Overall % (min – max)]), and user's accuracy of the wetland class ('Users.Acc.CV' [Overall % (min – max)]) are shown. All models were significant at p < 0.001.

SA	Date	PPT	n	OOB (%)	Random Forests model			Bootstrapped cross-validation		
					Prod. Acc. Mdl (%)	Users. Acc. Mdl (%)	kappa	PCC _p (%)	Prod. Acc. CV (%)	Users. Acc. CV (%)
SA1	12 Sep 2012	Dry	660	11.2 (9.4, 13.0)	90.5 (88.5–92.7)	86.7 (84.2–89.2)	0.78 (0.08)	89.1 (75.2–100)	90.8 (79.3–100)	87.0 (69.7–100)
SA1	5 May 2013	Moderate	660	4.2 (2.1, 6.4)	97.8 (96.8–98.9)	93.2 (92.3–94.6)	0.91 (0.03)	95.3 (86.0–100)	97.4 (88.9–100)	94.0 (78.8–100)
SA1	8 Jul 2011	Wet	660	3.3 (2.1, 4.6)	97.6 (96.0–98.3)	95.6 (94.9–96.6)	0.93 (0.02)	96.9 (87.6–100)	97.9 (90.9–100)	95.7 (87.9–100)
SA2	27 Sep 2012	Dry	920	15.0 (12.0, 18.0)	89.3 (87.6–91.4)	80.5 (78.5–83.6)	0.71 (0.07)	85.6 (70.2–95.6)	89.9 (80.0–100)	79.9 (63.0–93.5)
SA2	10 Jun 2013	Moderate	920	5.4 (4.1, 6.7)	95.6 (94.8–97.5)	92.8 (91.8–93.7)	0.89 (0.04)	94.4 (85.6–100)	95.4 (88.2–100)	92.7 (80.4–100)
SA2	3 Jun 2011	Wet	920	6.0 (3.0, 9.0)	96.9 (95.9–97.7)	91.7 (90.6–93.0)	0.89 (0.03)	94.5 (85.6–100)	97.0 (89.4–100)	92.7 (80.4–100)
SA3	22 Jul 2012	Dry	900	8.1 (5.1, 11.2)	94.6 (93.2–96.0)	88.3 (86.8–89.3)	0.83 (0.05)	92.1 (81.9–98.9)	95.5 (88.6–100)	88.8 (77.8–97.8)
SA3	26 Jul 2010	Moderate	900	5.9 (3.6, 8.3)	96.1 (94.8–97.1)	91.1 (89.8–92.3)	0.87 (0.03)	94.3 (83.3–98.9)	96.0 (87.5–100)	91.0 (82.2–100)
SA3	3 May 2011	Wet	900	3.4 (2.9, 4.0)	96.8 (96.0–97.7)	95.9 (95.0–96.8)	0.93 (0.02)	96.6 (90.9–100)	96.9 (90.0–100)	96.1 (88.9–100)
SA4	25 Jun 2012	Dry	1180	3.1 (1.9, 4.4)	98.1 (97.5–98.6)	95.7 (94.9–96.4)	0.94 (0.02)	97.4 (90.5–100)	98.3 (94.7–100)	95.9 (88.1–100)
SA4	8 Sep 2011	Moderate	1180	4.3 (2.5, 6.1)	97.2 (96.5–98.1)	93.8 (92.7–94.7)	0.91 (0.03)	95.7 (89.7–100)	97.2 (90.5–100)	93.8 (86.4–98.3)
SA4	30 Jul 2011	Wet	1180	3.2 (1.9, 4.6)	98.3 (97.9–98.8)	95.6 (95.1–96.8)	0.94 (0.02)	96.6 (91.4–100)	98.2 (93.3–100)	95.4 (86.4–100)

Table A2

Wetland prediction results for Landsat sampling areas ('SA') at three points in time across the growing season for six selected years using Random Forest (RF) models. 'PPT' indicates the relative amount of precipitation for the year classified and 'Season' represents the time within the growing season. For the Random Forests models, the following metrics are reported: Out-of-bag error ('OOB'; representative of model fit) [Total (non-wetland class, wetland class)], root-mean-square error ('RMSE'), producer's accuracy of the wetland class ('Prod.Acc.Mdl' [Overall % (min – max)]), user's accuracy of the wetland class ('Users.Acc.Mdl' [Overall % (min – max)]), and kappa (a measure of model specificity; [mean (diff. between min and max)]). For the bootstrapped cross-validations (n = 1000), percent correctly classified ('PCC_p'; representative of model performance [Mean (min – max)]), and producer's accuracy of the wetland class ('Prod.Acc.CV' [Overall % (min – max)]), and user's accuracy of the wetland class ('Users.Acc.CV' [Overall % (min – max)]) are shown. All models were significant at p < 0.001.

SA	Date	PPT	Season	OOB (%)	Random Forests model				Bootstrapped cross-validation		
					RMSE	Prod. Acc. Mdl (%)	Users. Acc. Mdl (%)	kappa	PCC _p (%)	Prod.Acc.CV (%)	Users. Acc. CV (%)
SA1	1 May 84	Med	Early	1.4 (0, 3.0)	0.118	76.5 (74.6–78.3)	72.0 (69.5–74.2)	0.53 (0.06)	76.5 (68.7–83.5)	79.2 (70.2–88.7)	72.1 (59.0–83.6)
SA1	20 Jul 84	Med	Mid	1.2 (0, 2.6)	0.109	78.1 (76.3–80.2)	75.5 (73.4–78.2)	0.57 (0.07)	78.6 (71.6–86.0)	80.6 (71.4–90.7)	75.3 (62.3–86.9)
SA1	21 Aug 84	Med	Late	1.3 (0, 2.8)	0.115	78.2 (76.7–80.1)	74.0 (71.9–76.2)	0.56 (0.05)	78.1 (69.5–87.6)	80.7 (72.0–89.8)	74.0 (59.8–86.9)
SA1	10 Apr 88	Dry	Early	1.2 (0, 2.6)	0.111	76.0 (73.9–77.9)	69.0 (67.0–72.2)	0.50 (0.07)	75.3 (67.0–83.9)	78.6 (70.3–88.1)	69.2 (52.5–81.0)
SA1	15 Jul 88	Dry	Mid	1.2 (0, 2.6)	0.109	82.1 (80.4–84.1)	75.0 (73.1–77.2)	0.61 (0.05)	80.2 (72.4–87.6)	84.3 (75.7–92.2)	75.1 (60.7–86.1)
SA1	1 Sep 88	Dry	Late	1.1 (0, 2.3)	0.103	78.0 (76.3–79.8)	73.3 (71.6–75.2)	0.56 (0.06)	77.3 (68.3–85.6)	80.2 (68.0–89.5)	73.2 (59.8–86.9)
SA1	10 May 93	Wet	Early	1.4 (0, 2.9)	0.116	82.5 (80.8–84.1)	78.0 (75.7–79.9)	0.64 (0.06)	81.9 (74.9–89.3)	84.5 (76.0–93.5)	78.2 (66.4–90.2)
SA1	29 Jul 93	Wet	Mid	0.9 (0, 1.9)	0.095	85.6 (84.0–87.6)	84.0 (82.4–85.7)	0.72 (0.05)	86.0 (79.4–93.0)	87.5 (79.5–96.5)	84.1 (73.0–91.8)
SA1	14 Aug 93	Wet	Late	1.0 (0, 2.2)	0.101	84.7 (83.0–86.2)	83.3 (81.7–85.0)	0.70 (0.05)	85.1 (78.6–93.0)	86.6 (79.5–99.1)	83.4 (69.7–92.6)
SA1	25 Apr 99	Med	Early	1.0 (0, 2.2)	0.101	86.4 (84.7–88.3)	81.6 (79.8–83.4)	0.71 (0.06)	85.1 (77.7–91.7)	88.1 (80.0–96.3)	81.8 (71.3–92.6)
SA1	14 Jul 99	Med	Mid	1.1 (0, 2.3)	0.103	89.4 (87.7–90.8)	83.8 (82.5–85.3)	0.75 (0.05)	87.6 (80.6–92.6)	90.7 (83.2–98.1)	83.8 (72.1–92.6)
SA1	16 Sep 99	Med	Late	1.5 (0, 3.2)	0.122	86.6 (85.0–88.2)	82.5 (80.9–84.3)	0.72 (0.05)	85.6 (77.7–91.7)	88.1 (78.8–96.0)	82.6 (72.1–91.8)
SA1	19 May 02	Dry	Early	1.0 (0, 2.2)	0.101	82.3 (80.8–83.9)	77.4 (75.7–79.5)	0.63 (0.06)	81.4 (72.8–88.4)	84.3 (76.0–93.1)	77.4 (65.6–88.5)
SA1	6 Jul 02	Dry	Mid	0.8 (0, 1.8)	0.091	81.6 (80.0–83.2)	79.7 (78.0–81.7)	0.64 (0.05)	81.9 (75.7–88.9)	83.6 (75.2–92.2)	79.6 (67.2–90.2)
SA1	23 Aug 02	Dry	Late	0.6 (0, 1.3)	0.079	81.9 (80.2–83.3)	79.1 (76.6–80.8)	0.64 (0.06)	81.9 (74.0–89.3)	83.8 (73.7–93.5)	79.3 (68.9–90.2)
SA1	15 Jul 11	Wet	Mid	0.6 (0, 1.3)	0.079	93.2 (92.3–94.3)	90.4 (89.3–91.7)	0.85 (0.04)	92.2 (85.6–97.1)	94.1 (86.0–100)	90.3 (81.1–96.7)

(continued on next page)

Table A2 (continued)

SA	Date	PPT	Season	OOB (%)	Random Forests model				Bootstrapped cross-validation		
					RMSE	Prod. Acc. Mdl (%)	Users. Acc. Mdl (%)	kappa	PCC _p (%)	Prod.Acc.CV (%)	Users. Acc. CV (%)
SA1	16 Aug 11	Wet	Late	0.7 (0, 1.2)	0.081	89.9 (88.7–91.2)	84.9 (83.4–86.2)	0.77 (0.04)	88.4 (82.7–94.6)	91.2 (84.5–97.4)	85.0 (75.4–93.4)
SA2	23 May 84	Med	Early	1.0 (0, 2.1)	0.101	95.2 (94.2–96.3)	86.8 (85.6–87.9)	0.82 (0.03)	91.0 (85.2–95.2)	95.4 (89.2–99.2)	86.9 (79.5–95.9)
SA2	27 Aug 84	Med	Late	1.1 (0, 2.3)	0.106	92.9 (91.7–94.2)	83.7 (82.4–84.9)	0.77 (0.03)	88.6 (83.1–93.5)	93.1 (86.2–98.4)	83.8 (71.9–93.2)
SA2	5 Jul 88	Dry	Mid	0.9 (0, 1.8)	0.094	89.3 (88.0–90.8)	81.9 (80.4–83.4)	0.72 (0.05)	85.9 (80.4–92.8)	89.4 (82.6–97.0)	81.9 (71.2–90.4)
SA2	22 Aug 88	Dry	Late	0.9 (0, 1.7)	0.092	85.8 (84.5–87.2)	82.3 (80.8–83.7)	0.69 (0.05)	84.5 (77.3–90.0)	86.0 (78.2–95.4)	82.3 (71.2–91.8)
SA2	16 May 93	Wet	Early	1.2 (0, 2.3)	0.108	95.9 (95.1–96.5)	88.4 (87.3–89.5)	0.85 (0.03)	92.4 (87.9–95.9)	96.0 (90.3–100)	88.4 (77.4–95.9)
SA2	4 Aug 93	Wet	Late	1.2 (0, 2.5)	0.111	93.7 (92.7–94.9)	85.0 (83.5–86.1)	0.79 (0.05)	89.7 (84.5–94.5)	93.7 (87.2–99.2)	85.0 (74.7–93.8)
SA2	1 May 99	Med	Early	1.1 (0, 2.3)	0.106	93.8 (92.8–95.0)	86.5 (85.3–87.6)	0.81 (0.03)	90.4 (84.8–94.1)	94.0 (87.5–99.2)	86.6 (76.0–95.2)
SA2	6 Sep 99	Med	Late	0.8 (0, 1.7)	0.091	94.1 (93.0–95.1)	89.1 (88.2–90.3)	0.84 (0.03)	91.7 (87.3–96.6)	94.2 (88.3–99.2)	89.2 (80.8–95.9)
SA2	25 May 02	Dry	Early	1.0 (0, 2.1)	0.101	93.6 (92.6–94.8)	85.8 (84.6–86.8)	0.80 (0.04)	90.0 (83.1–94.5)	93.7 (85.2–99.2)	85.7 (77.4–94.5)
SA2	14 Sep 02	Dry	Late	1.2 (0, 2.5)	0.111	84.7 (83.3–86.3)	80.7 (79.4–82.2)	0.66 (0.05)	83.1 (76.6–89.0)	84.9 (77.3–91.8)	80.9 (68.5–91.1)
SA2	7 Sep 11	Wet	Late	1.2 (0, 2.4)	0.109	94.8 (94.0–95.7)	89.2 (88.1–90.2)	0.57 (0.07)	92.4 (86.9–96.6)	94.9 (89.0–99.3)	89.3 (80.1–96.6)
SA3	16 May 84	Med	Early	0.7 (0, 1.3)	0.082	77.4 (76.0–78.8)	73.2 (71.6–75.1)	0.51 (0.05)	75.5 (67.2–82.9)	77.1 (68.5–85.9)	73.1 (58.3–84.6)
SA3	3 Jul 84	Med	Mid	0.5 (0, 0.9)	0.067	68.9 (67.2–70.6)	66.6 (64.2–68.7)	0.36 (0.05)	67.8 (59.8–75.2)	68.5 (60.4–77.7)	66.7 (55.1–78.8)
SA3	5 Sep 84	Med	Late	0.5 (0, 1.0)	0.072	68.1 (66.7–77.1)	67.6 (65.5–69.8)	0.35 (0.07)	67.5 (59.8–76.5)	67.8 (58.7–78.6)	67.8 (53.8–76.9)
SA3	27 May 88	Dry	Early	0.7 (0, 1.5)	0.086	69.9 (67.8–71.5)	67.9 (65.2–70.0)	0.38 (0.07)	69.1 (60.4–95.0)	69.7 (60.9–80.8)	68.1 (51.9–78.8)
SA3	15 Aug 88	Dry	Late	0.4 (0, 0.8)	0.062	66.2 (64.5–68.1)	63.9 (61.9–66.1)	0.31 (0.06)	65.2 (58.5–75.5)	65.9 (57.8–75.4)	64.1 (50.6–75.6)
SA3	25 May 93	Wet	Early	0.6 (0, 1.2)	0.078	77.2 (75.8–79.0)	72.7 (70.8–74.3)	0.51 (0.06)	75.2 (66.9–82.6)	76.9 (69.3–87.0)	72.4 (60.9–82.1)
SA3	24 Apr 99	Med	Early	1.0 (0, 2.0)	0.101	87.7 (86.6–88.9)	85.8 (84.5–87.1)	0.73 (0.04)	86.8 (80.0–92.3)	87.6 (79.3–95.1)	86.0 (77.6–94.2)
SA3	13 Jul 99	Med	Mid	0.7 (0, 1.3)	0.082	88.5 (87.2–89.8)	80.8 (79.7–82.1)	0.70 (0.04)	84.9 (78.7–90.7)	88.2 (81.4–94.9)	80.9 (69.9–90.4)
SA3	14 Aug 99	Med	Late	1.3 (0, 2.6)	0.115	87.6 (86.1–88.8)	83.5 (82.1–85.0)	0.71 (0.03)	85.8 (79.4–91.0)	87.4 (78.1–95.1)	83.5 (73.7–93.6)
SA3	18 May 02	Dry	Early	1.2 (0, 2.3)	0.108	85.5 (84.1–86.8)	81.5 (80.0–83.0)	0.67 (0.04)	84.0 (76.5–89.0)	85.3 (76.4–92.6)	81.5 (68.6–92.3)
SA3	5 Jul 02	Dry	Mid	0.7 (0, 1.4)	0.084	83.9 (82.5–85.5)	75.7 (74.2–77.5)	0.61 (0.04)	80.4 (73.6–87.1)	83.7 (76.2–91.1)	75.7 (64.1–86.5)
SA3	7 Sep 02	Dry	Late	0.7 (0, 1.5)	0.086	85.3 (83.7–87.0)	73.1 (71.5–74.8)	0.60 (0.06)	80.0 (73.3–86.5)	85.3 (77.4–93.3)	73.3 (63.5–85.3)
SA4	14 Apr 84	Med	Early	1.2 (0.1, 2.3)	0.108	90.0 (89.2–91.2)	90.8 (89.8–91.9)	0.81 (0.04)	90.3 (84.6–95.6)	90.0 (82.1–96.1)	90.8 (83.8–96.2)
SA4	19 Jul 84	Med	Mid	0.7 (0, 1.4)	0.085	89.5 (88.7–90.4)	91.1 (90.1–92.3)	0.80 (0.03)	90.3 (85.6–95.3)	89.5 (82.7–95.6)	91.1 (84.4–98.8)
SA4	27 May 88	Dry	Early	0.7 (0.3, 1.1)	0.083	91.8 (90.8–92.7)	90.9 (89.9–91.9)	0.83 (0.03)	91.5 (85.9–96.2)	91.8 (85.7–97.4)	90.8 (83.1–96.9)
SA4	30 Jul 88	Dry	Mid	0.8 (0.1, 1.5)	0.088	91.9 (90.9–93.2)	88.8 (87.8–90.2)	0.81 (0.04)	90.6 (85.2–95.0)	91.9 (86.1–97.8)	88.7 (80.0–95.6)
SA4	30 Sep 93	Wet	Late	1.2 (0, 2.4)	0.110	90.5 (89.4–91.7)	88.9 (87.8–89.9)	0.80 (0.03)	90.0 (83.4–95.0)	90.5 (84.0–96.7)	88.8 (78.8–96.9)
SA4	26 May 99	Med	Early	0.8 (0.3, 1.2)	0.087	90.8 (90.0–91.7)	93.2 (92.1–94.0)	0.84 (0.03)	91.8 (86.5–95.6)	90.7 (84.7–96.7)	93.2 (86.9–97.5)
SA4	13 Jul 99	Med	Mid	0.5 (0.1, 0.9)	0.073	91.2 (90.3–92.1)	93.4 (92.4–94.2)	0.84 (0.03)	92.1 (86.8–95.6)	91.2 (85.5–96.8)	93.2 (86.2–98.8)
SA4	18 May 02	Dry	Early	0.7 (0, 1.4)	0.083	91.6 (90.9–92.4)	92.5 (91.7–93.5)	0.84 (0.02)	92.1 (87.4–96.2)	91.7 (85.8–98.0)	92.6 (85.0–97.5)
SA4	7 Sep 02	Dry	Late	0.7 (0.1, 1.4)	0.085	91.4 (90.6–92.3)	93.3 (92.2–94.4)	0.85 (0.03)	92.1 (87.1–95.9)	91.4 (84.4–96.8)	93.3 (85.6–98.1)
SA4	25 Apr 11	Wet	Early	0.8 (0, 1.5)	0.087	92.7 (91.8–93.8)	91.7 (90.7–92.5)	0.84 (0.03)	92.1 (88.7–97.2)	92.7 (86.5–99.3)	91.7 (85.0–98.1)
SA4	28 Jun 11	Wet	Mid	0.5 (0, 0.9)	0.069	92.6 (91.8–93.8)	92.3 (91.5–93.6)	0.85 (0.03)	92.5 (87.1–98.1)	92.7 (86.0–98.0)	92.3 (84.4–98.8)
SA4	16 Sep 11	Wet	Late	0.4 (0, 0.9)	0.066	91.4 (90.2–92.3)	92.6 (91.7–93.7)	0.84 (0.03)	91.8 (87.8–95.6)	91.5 (86.0–98.6)	92.5 (81.9–98.1)

evaluated by difference in sensitivity-specificity exemplified for Landsat models in SA3. The vertical line marks the position of the 0.65 wetland probability threshold. Difference in sensitivity-specificity is the threshold evaluation metric recommended by Jimenez-Valverde & Lobo (2007).

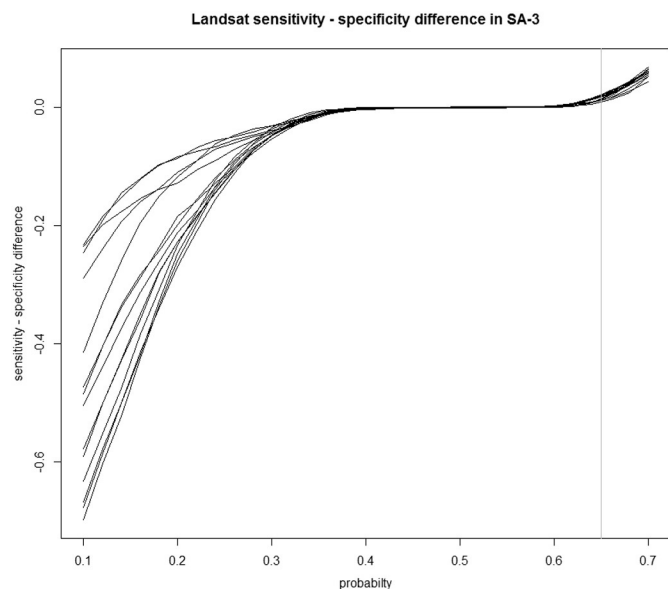


Fig. A1 Sensitivity analysis of different probability thresholds

References

- Agassiz National Wildlife Refuge, 2005. *Comprehensive Conservation Plan*.
- Augusteijn, M.F., Warrender, C.E., 1998. Wetland classification using optical and radar data and neural network classification. *Int. J. Remote Sens.* 19 (8), 1545–1560. <http://dx.doi.org/10.1080/014311698215342>.
- Baker, C., Lawrence, R., Montagne, C., Patten, D., 2006. Mapping wetlands and riparian areas using Landsat ETM+ imagery and decision-tree-based models. *Wetlands* 26 (2), 465–474. [http://dx.doi.org/10.1672/0277-5212\(2006\)26\[465:MWARAU\]2.0.CO;2](http://dx.doi.org/10.1672/0277-5212(2006)26[465:MWARAU]2.0.CO;2).
- Ballard, T., Seager, R., Smerdon, J.E., Cook, B.L., Ray, A.J., Rajagopalan, B., ... Henderson, N., 2014. Hydroclimate variability and change in the Prairie Pothole Region, the “Duck Factory” of North America. *Earth Interactions* 18 (14), 1–28. <http://dx.doi.org/10.1175/EI-D-14-0004.1>.
- Beeri, O., Phillips, R., 2007. Tracking palustrine water seasonal and annual variability in agricultural wetland landscapes using Landsat from 1997 to 2005. *Global Change Biology* 13, 897–912 (Retrieved from papers://6a81516e-e118-490c-85ce-527bd8959a94/Paper/p1689).
- Biau, G., 2012. Analysis of a random forests model. *J. Mach. Learn. Res.* 13, 1063–1095 (Retrieved from <http://arxiv.org/abs/1005.0208>).
- Bolen, E.G., Smith, L.M., Schramm, H.L., 1989. Playa lakes: prairie wetlands of the southern High Plains. *BioScience* 39 (9), 615–623. <http://dx.doi.org/10.2307/1.311.091>.
- Bourgeau-Chavez, L.L., Riordan, K., Powell, R.B., Miller, N., Nowels, M., 2009. Improving wetland characterization with multi-sensor, multi-temporal SAR and optical/infrared data fusion. *Adv. Geosci. Remote Sens.* 679–708.
- Breiman, L., 2001. Statistical modeling: the two cultures. *Stat. Sci.* 16 (3), 199–231. <http://dx.doi.org/10.2307/2676681>.
- Bwangoy, J.-R.B., Hansen, M.C., Roy, D.P., De Grandi, G., Justice, C.O., 2009. Wetland mapping in the Congo Basin using optical and radar remotely sensed data and derived topographical indices. *Remote Sens. Environ.* 114 (1), 73–86. <http://dx.doi.org/10.1016/j.rse.2009.08.004>.
- Carpenter, S.R., DeFries, R., Dietz, T., Mooney, H.A., Polasky, S., Reid, W.V., Scholes, R.J., 2006. Millennium ecosystem assessment: research needs. *Science* 314, 257–258. <http://dx.doi.org/10.1126/science.1131946>.
- Chavez, P.S., 1988. An improved dark-object subtraction technique for atmospheric scattering correction of multispectral data. *Remote Sens. Environ.* 24 (3), 459–479. [http://dx.doi.org/10.1016/0034-4257\(88\)90019-3](http://dx.doi.org/10.1016/0034-4257(88)90019-3).

- Chavez, P.S.J., 1996. Image-based atmospheric corrections-revisited and improved. *Photogramm. Eng. Remote Sens.* 62 (9), 1025–1036 (doi:0099-1112/96/6209-1025).
- Compton, B.W., McGarigal, K., Cushman, S.A., Gamble, L.R., 2007. A resistant-kernel model of connectivity for amphibians that breed in vernal pools. *Conserv. Biol.* 21 (3), 788–799. <http://dx.doi.org/10.1111/j.1523-1739.2007.00674.x>.
- Congalton, R.G., Jones, R., Schrie, J., 2002. Evaluating remotely sensed techniques for mapping riparian vegetation. *Comput. Electron. Agric.* 37, 113–126.
- Conly, F.M., van der Kamp, G., 2001. Monitoring the hydrology of Canadian prairie wetlands to detect the effects of climate change and land use changes. *Environ. Monit. Assess.* 67, 195–215 (Retrieved from <http://www.ncbi.nlm.nih.gov/pubmed/11339699>).
- Cowardin, L.M., 1982. Some conceptual and semantic problems in wetland classification and inventory. *Wildl. Soc. Bull.* 10 (1), 57–60.
- Cowardin, L.M., Carter, V., Golet, F.C., LaRoe, E.T., 1979. *Classification of Wetlands and Deepwater habitats of the United States*. Washington, D.C.
- Cowardin, L.M., Golet, F.C., 1995. US fish and Wildlife Service 1979 wetland classification: a review. *Vegetatio* 118, 139–152.
- Cushman, S.A., Evans, J.S., McGarigal, K., Kiesecker, J.M., 2010. Toward Gleasonian Landscape Ecology: From Communities to Species, from Patches to Pixels. Department of Agriculture, Forest Service, Rocky Mountain Research Station, Fort Collins, CO: U.S. (Retrieved from <http://www.scopus.com/inward/record.url?eid=2-s2.0-78650576120&partnerID=40&md5=1aa7d8d0ee6e211f11cc08eb79ca3cdc>).
- Cutler, D.R., Edwards, T.C., Beard, K.H., Cutler, A., Hess, K.T., Gibson, J., Lawler, J.J., 2007. Random forests for classification in ecology. *Ecology* 88 (11), 2783–2792 (Retrieved from <http://www.ncbi.nlm.nih.gov/pubmed/18051647>).
- Dale, P.E.R., Connelly, R., 2012. Wetlands and human health: an overview. *Wetl. Ecol. and Manag.* 20 (3), 165–171. <http://dx.doi.org/10.1007/s11273-012-9264-4>.
- Daniels, A.E., 2006. Incorporating domain knowledge and spatial relationships into land cover classifications: a rule-based approach. *Int. J. Remote Sens.* 27 (14), 2949–2975. <http://dx.doi.org/10.1080/01431160600567753>.
- De Fries, R.S., Hansen, M., Townshend, J.R.G., Sohlberg, R., 1998. Global land cover classifications at 8 km spatial resolution: the use of training data derived from Landsat imagery in decision tree classifiers. *Int. J. Remote Sens.* 19 (16), 3141–3168. <http://dx.doi.org/10.1080/014311698214235>.
- Elphick, C.S., 2000. Functional equivalency between rice fields and seminatural wetland habitats. *Conserv. Biol.* 14 (1), 181–191. <http://dx.doi.org/10.1046/j.1523-1739.2000.98314.x>.
- Euliss, N.H., LaBaugh, J.W., Fredrickson, L.H., Mushet, D.M., Laubhan, M.K., Swanson, G.A., ... Nelson, R.D., 2004. The wetland continuum: a conceptual framework for interpreting biological studies. *Wetlands* 24 (2), 448–458. [http://dx.doi.org/10.1672/0277-5212\(2004\)024\[0448:TWACAF\]2.0.CO;2](http://dx.doi.org/10.1672/0277-5212(2004)024[0448:TWACAF]2.0.CO;2).
- Euliss, N.H., Mushet, D., Wrubleski, D.A., 1999. *Wetlands of the Prairie Pothole Region: Invertebrate species composition, ecology, and management*. In: Batzer, D., Rader, R., Wissinger, S. (Eds.), *Invertebrates in Freshwater Wetlands of North America: Ecology and Management*. Bozeman: John Wiley & Sons, pp. 471–514.
- Evans, J., Cushman, S., 2009. Gradient modeling of conifer species using random forests. *Landscape Ecol.* 24 (5), 673–683.
- Evans, J.S., & Murphy, M.A. (2015). Package “rUtilities.” R package (Vol. 1.0–1).
- Evans, J.S., Murphy, M.A., Holden, Z.A., Cushman, S.A., 2011. Modeling species distribution and change using Random Forest. In: Drew, C.A., Wiersma, Y.F., Huettmann, F. (Eds.), *Predictive Species and Habitat Modeling in Landscape Ecology: Concepts and Applications*. Springer New York, New York, NY, pp. 139–159 <http://dx.doi.org/10.1007/978-1-4419-7390-0>.
- Evans, T.L., Costa, M., Tomas, W.M., Camilo, A.R., 2014. Large-scale habitat mapping of the Brazilian Pantanal wetland: a synthetic aperture radar approach. *Remote Sens. Environ.* 155, 89–108. <http://dx.doi.org/10.1016/j.rse.2013.08.051>.
- Finlayson, C.M., van der Valk, A.G., 1995. *Wetland classification and inventory: a summary*. *Vegetation* 118, 185–192.
- Folke, C., Carpenter, S., Walker, B., Scheffer, M., Elmqvist, T., Gunderson, L., Holling, C.S., 2004. Regime shifts, resilience, and biodiversity in ecosystem management. *Annu. Rev. Ecol. Syst.* 35, 557–581. <http://dx.doi.org/10.2307/annurev.ecolsys.35.021103.30000021>.
- Gallant, A., 2015. The challenges of remote monitoring of wetlands. *Remote Sens.* 7 (8), 10938–10950. <http://dx.doi.org/10.3390/rs70810938>.
- Geerling, G.W., Labrador-García, M., Clevers, J.G.P.W., Ragas, A.M.J., Smits, A.J.M., 2007. Classification of floodplain vegetation by data fusion of spectral (CASI) and LiDAR data. *Int. J. Remote Sens.* 28 (19), 4263–4284. <http://dx.doi.org/10.1080/01431160701241720>.
- Gibbs, J.P., 2000. Wetland loss and biodiversity conservation. *Conserv. Biol.* 14 (1), 314–317. <http://dx.doi.org/10.1046/j.1523-1739.2000.98608.x>.
- Gleason, R.A., Laubhan, M.K., Euliss, N.H., 2008. *Ecosystem Services Derived from Wetland Conservation Practices in the United States Prairie Pothole Region with an Emphasis on the US Department of Agriculture Conservation Reserve and Wetlands Reserve Programs*. Reston, VA.
- Gómez-Rodríguez, C., Bustamante, J., Díaz-Paniagua, C., 2010. Evidence of hydroperiod shortening in a preserved system of temporary ponds. *Remote Sens.* 2 (6), 1439–1462. <http://dx.doi.org/10.3390/rs2061439>.
- Gondwe, B.R.N., Hong, S.H., Wdowinski, S., Bauer-Gottwein, P., 2010. Hydrologic dynamics of the ground-water-dependent San Ka'an wetlands, Mexico, derived from InSAR and SAR data. *Wetlands* 30 (1), 1–13. <http://dx.doi.org/10.1007/s13157-009-0016-z>.
- Gosz, J.R., 1992. Gradient analysis of ecological change in time and space: implications for forest management. *Ecol. Appl.* 2 (3), 248–261. <http://dx.doi.org/10.2307/1,941,859>.
- Hastie, T., Tibshirani, R., Friedman, J.H., 2001. *The Elements of Statistical Learning: Data Mining, Inference, and Prediction*. Springer Series in Statistics, New York, NY <http://dx.doi.org/10.1007/978-0-387-84858-7>.
- Hay, G.J., Dube, P., Bouchard, A., Marceau, D.J., 2002. A scale-space primer for exploring and quantifying complex landscapes. *Ecol. Model.* 153, 27–49.
- Hijmans, R.J., van Etten, J., Mattiuzzi, M., Sumner, M., Greenberg, J.A., Lamigueiro, O.P., ... Shortridge, A., 2014. Package “raster.” R (Retrieved from <http://cran.r-project.org/web/packages/raster/raster.pdf>).
- Horwitz, P., Finlayson, C.M., 2011. Wetlands as settings for human health: incorporating ecosystem services and health impact assessment into water resource management. *BioScience* 61 (9), 678–688. <http://dx.doi.org/10.1525/bio.2011.61.9.6>.
- Huang, C., Peng, Y., Lang, M., Yeo, I.-Y., McCarty, G., 2014. Wetland inundation mapping and change monitoring using Landsat and airborne LiDAR data. *Remote Sens. Environ.* 141, 231–242. <http://dx.doi.org/10.1016/j.rse.2013.10.020>.
- Huang, C., Wylie, B., Yang, L., Homer, C., Zylstra, G., 2002. Derivation of a tasseled cap transformation based on Landsat 7 at-satellite reflectance. *Int. J. of Remote Sens.* 23, 1741–1748. <http://dx.doi.org/10.1080/01431160110106113>.
- Hudak, A.T., Lefsky, M.A., Cohen, W.B., Berterretche, M., 2002. Integration of lidar and Landsat ETM+ data for estimating and mapping forest canopy height. *Remote Sens. Environ.* 82, 397–416. [http://dx.doi.org/10.1016/S0034-4257\(02\)00056-1](http://dx.doi.org/10.1016/S0034-4257(02)00056-1).
- Huete, A.R., 1988. A soil-adjusted vegetation index (SAVI). *Remote Sens. Environ.* 25, 295–309. [http://dx.doi.org/10.1016/0034-4257\(88\)90106-X](http://dx.doi.org/10.1016/0034-4257(88)90106-X).
- Hurlbert, S., 1984. Pseudoreplication and the design of ecological field experiments. *Ecol. Monogr.* 54 (2), 187–211.
- Jackson, C., 2006. *Wetland hydrology*. In: Batzer, D., Sharitz, R. (Eds.), *Ecology of Freshwater and Estuarine Wetlands*. University of California Press, Berkeley, pp. 43–81.
- Jiménez-Valverde, A., Lobo, J.M., 2007. Threshold criteria for conversion of probability of species presence to either-or presence-absence. *Acta Oecol.* 31 (3), 361–369. <http://dx.doi.org/10.1016/j.actao.2007.02.001>.
- Johansen, K., Coops, N.C., Gergel, S.E., Stange, Y., 2007. Application of high spatial resolution satellite imagery for riparian and forest ecosystem classification. *Remote Sens. Environ.* 110, 29–44. <http://dx.doi.org/10.1016/j.rse.2007.02.014>.
- Johnson, D.M., 2013. A 2010 map estimate of annually tilled cropland within the conterminous United States. *Agric. Syst.* 114, 95–105. <http://dx.doi.org/10.1016/j.agry.2012.08.004>.
- Johnson, W.C., Boettcher, S.E., Poiani, K.A., Guntenspergen, G.R., 2004. Influence of weather extremes on the water levels of glaciated prairie wetlands. *Wetlands* 24 (2), 385–398.
- Johnson, W.C., Millett, B., Gilmanov, T., Voldseth, R., Guntenspergen, G., Naugle, D., 2005. Vulnerability of northern prairie wetlands to climate change. *BioScience* 55 (10), 863–872.
- Johnson, W.C., Werner, B., Guntenspergen, G.R., Voldseth, R.A., Millett, B., Naugle, D.E., ... Olawsky, C., 2010. Prairie wetland complexes as landscape functional units in a changing climate. *BioScience* 60 (2), 128–140. <http://dx.doi.org/10.1525/bio.2010.60.2.7>.
- Ju, J., Gopal, S., Kolaczyk, E.D., 2005. On the choice of spatial and categorical scale in remote sensing land cover classification. *Remote Sens. Environ.* 96 (1), 62–77. <http://dx.doi.org/10.1016/j.rse.2005.01.016>.
- Kahara, S.N., Mockler, R.M., Higgins, K.F., Chipps, S.R., Johnson, R.R., 2009. Spatiotemporal patterns of wetland occurrence in the Prairie Pothole Region of eastern South Dakota. *Wetlands* 29 (2), 678–689.
- Kantrud, H.A., Krapu, G.L., Swanson, G.A., Allen, J.A., 1989. *Prairie Basin Wetlands of the Dakotas: A Community Profile*.
- Knight, J.F., Tolcser, B.P., Corcoran, J.M., Rampi, L.P., 2013. The effects of data selection and thematic detail on the accuracy of high spatial resolution wetland classifications. *Photogramm. Eng. Remote Sens.* 79 (7), 613–623. <http://dx.doi.org/10.14358/PERS.79.7.613>.
- Kruskal, J.B., 1964. Nonmetric multidimensional scaling: a numerical method. *Psychometrika* 29 (2), 115–129.
- Lang, M., Kasischke, E., Prince, S., Pittman, K., 2008. Assessment of C-band synthetic aperture radar data for mapping and monitoring Coastal Plain forested wetlands in the Mid-Atlantic Region, USA. *Remote Sens. Environ.* 112 (11), 4120–4130.
- Li, C., Cutler, A., 2013. *Probability Estimation in Random Forests*.
- Li, J., Chen, W., 2005. A rule-based method for mapping Canada's wetlands using optical, radar and DEM data. *Int. J. Remote Sens.* 26 (22), 5051–5069. <http://dx.doi.org/10.1080/01431160500166516>.
- Liaw, A., Wiener, M., 2002. Classification and regression by Random Forest. *R News* 2 (December), 18–22. <http://dx.doi.org/10.1177/154405910408300516>.
- Liu, G., Schwartz, F., 2012. Climate-driven variability in lake and wetland distribution across the Prairie Pothole Region: From modern observations to long-term reconstructions with space-for-time substitution. *Water Resour. Res.* 48 (8), W08526.
- Lortie, C.J., Brooker, R.W., Choler, P., Kikvidze, Z., Michalet, R., Pugnaire, F.I., Callaway, R.M., 2004. Rethinking plant community theory. *Oikos* 107 (2), 433–438. <http://dx.doi.org/10.1111/j.0030-1299.2004.13250.x>.
- Manning, A.D., Lindenmayer, D.B., Nix, H.A., 2004. Continua and umwelt: novel perspectives on viewing landscapes. *Oikos* 104 (3), 621–628. <http://dx.doi.org/10.1111/j.0030-1299.2004.12813.x>.
- Maxa, M., Bolstad, P., 2009. Mapping northern wetlands with high resolution satellite images and LiDAR. *Wetlands* 29 (1), 248–260. <http://dx.doi.org/10.1672/08-91.1>.
- McGarigal, K., Tagil, S., Cushman, S.A., 2009. Surface metrics: an alternative to patch metrics for the quantification of landscape structure. *Landscape Ecol.* 24, 433–450. <http://dx.doi.org/10.1007/s10980-009-9327-y>.
- McIntyre, S., Barrett, G.W., 1992. *Habitat variegation, an alternative to fragmentation*. *Conserv. Biol.* 6 (1), 146–147.
- Melendez-Pastor, I., Navarro-Pedreño, J., Koch, M., Gómez, I., 2010. Multi-resolution and temporal characterization of land-use classes in a Mediterranean wetland with land-cover fractions. *Int. J. Remote Sens.* 31 (20), 5365–5389. <http://dx.doi.org/10.1080/01431160903349065>.

- Murphy, M., Evans, J., Storfer, A., 2010. Quantifying *Bufo boreas* connectivity in Yellowstone National Park with landscape genetics. *Ecology* 91 (1), 252–261.
- Niemuth, N.D., Wangler, B., Reynolds, R.E., 2010. Spatial and temporal variation in wet area of wetlands in the Prairie Pothole Region of North Dakota and South Dakota. *Wetlands* 30, 1053–1064. <http://dx.doi.org/10.1007/s13157-010-0111-1>.
- NOAA, 2013. National Centers for Environmental Information, Climate at a Glance Time Series. <http://www.ncdc.noaa.gov/cag/>.
- Ojima, D.S., Lockett, J.M., 2002. Preparing for a Changing Climate: The Potential Consequences of Climate Variability and Change - Central Great Plains Report for the US Global Change Research Program.
- Olson, D.M., Dinerstein, E., Wikramanayake, E.D., Burgess, N.D., Powell, G.V.N., Underwood, E.C., ... Kassem, K.R., 2001. Terrestrial ecoregions of the world: a new map of life on earth. *BioScience* 51 (11), 933–938. [http://dx.doi.org/10.1641/0006-3568\(2001\)051\[0933:TEOTWA\]2.0.CO;2](http://dx.doi.org/10.1641/0006-3568(2001)051[0933:TEOTWA]2.0.CO;2).
- Ozesmi, S.L., Bauer, M.E., 2002. Satellite remote sensing of wetlands. *Wetl. Ecol. Manag.* 10 (5), 381–402.
- Pavri, F., Aber, J., 2004. Characterizing wetland landscapes: a spatiotemporal analysis of remotely sensed data at Cheyenne Bottoms, Kansas. *Phys. Geogr.* 25 (1), 86–104. <http://dx.doi.org/10.2747/0272-3646.25.1.86>.
- Pickens, B.A., King, S.L., 2014. Linking multi-temporal satellite imagery to coastal wetland dynamics and bird distribution. *Ecol. Model.* 285, 1–12. <http://dx.doi.org/10.1016/j.ecolmodel.2014.04.013>.
- Qi, J., Chehbouni, A., Huete, A.R., Kerr, Y.H., Sorooshian, S., 1994. A modified soil adjusted vegetation index. *Remote Sensing of Environment* 48, 119–126. [http://dx.doi.org/10.1016/0034-4257\(94\)90134-1](http://dx.doi.org/10.1016/0034-4257(94)90134-1).
- Rover, J., Wright, C., Euliss, N., Mushet, D., Wylie, B., 2011. Classifying the hydrologic function of prairie potholes with remote sensing and GIS. *Wetlands* 31 (2), 319–327.
- Sabo, J.L., Sponseller, R., Dixon, M., Gabe, K., Harms, T., Heffernan, J., ... Welter, J., 2005. Riparian zones increase regional species richness by harboring different, not more, species: comment. *Ecology* 86 (1), 56–62 (Retrieved from <http://www.ncbi.nlm.nih.gov/pubmed/16937652>).
- Schuster, C., Förster, M., Kleinschmit, B., 2012. Testing the red edge channel for improving land-use classifications based on high-resolution multi-spectral satellite data. *Int. J. Remote Sens.* 30 (17), 5583–5599.
- Scott, D.A., Jones, T.A., 1995. Classification and inventory of wetlands : a global overview. *Vegetation* 118 (1), 3–16.
- Shaver, G.R., Canadell, J., Chapin, F.S., Gurevitch, J., Harte, J., Henry, G., ... Rustad, L., 2000. Global warming and terrestrial ecosystems: a conceptual framework for analysis. *BioScience* 50 (10), 871–882.
- Somers, B., Asner, G.P., Tits, L., Coppin, P., 2011. Endmember variability in spectral mixture analysis: a review. *Remote Sens. Environ.* 115 (7), 1603–1616. <http://dx.doi.org/10.1016/j.rse.2011.03.003>.
- Song, C., Woodcock, C., Seto, K., Lenney, M., Macomber, S., 2001. Classification and change detection using Landsat TM Data- when and how to correct atmospheric effects? *Remote Sens. Environ.* 75 (00), 230–244. [http://dx.doi.org/10.1016/S0034-4257\(00\)00169-3](http://dx.doi.org/10.1016/S0034-4257(00)00169-3).
- Sorenson, L.G., Goldberg, R., Root, T.L., Anderson, M.G., 1998. Potential effects of global warming on waterfowl populations breeding in the northern Great Plains. *Clim. Chang.* 40, 342–369.
- Soykan, C.U., Brand, L.A., Ries, L., Stromberg, J.C., Hass, C., Simmons, D.A., ... Sabo, J.L., 2012. Multitaxonomic diversity patterns along a desert riparian-upland gradient. *PLoS ONE* 7 (1), e28235. <http://dx.doi.org/10.1371/journal.pone.0028235>.
- Töyrä, J., Pietroniro, A., 2005. Towards operational monitoring of a northern wetland using geomatics-based techniques. *Remote Sens. Environ.* 97 (2), 174–191. <http://dx.doi.org/10.1016/j.rse.2005.03.012>.
- Töyrä, J., Pietroniro, A., Martz, L.W., 2001. Multisensor hydrologic assessment of a freshwater wetland. *Remote Sens. Environ.* 75 (2), 162–173. [http://dx.doi.org/10.1016/S0034-4257\(00\)00164-4](http://dx.doi.org/10.1016/S0034-4257(00)00164-4).
- van der Kamp, G., Hayashi, M., 1998. The groundwater recharge function of small wetlands in the semi-arid northern prairies. *Great Plains Res.* 8, 39–56 (Retrieved from <http://digitalcommons.unl.edu/greatplainsresearch/366/>).
- van der Valk, A.G., 2005. Water-level fluctuations in North American prairie wetlands. *Hydrobiologia* 539 (1), 171–188. <http://dx.doi.org/10.1007/s10750-004-4866-3>.
- Vanderbilt, V.C., Khanna, S., Ustin, S.L., 2007. Impact of pixel size on mapping surface water in subsolar imagery. *Remote Sens. Environ.* 109 (1), 1–9. <http://dx.doi.org/10.1016/j.rse.2006.12.009>.
- Werner, B.A., Johnson, W.C., Guntenspergen, G.R., 2013. Evidence for 20th century climate warming and wetland drying in the North American Prairie Pothole Region. *Ecol. Evol.* 3 (10), 3471–3482. <http://dx.doi.org/10.1002/ece3.731>.
- Wilén, B.O., Bates, M.K., 1995. The US Fish and Wildlife Service's National Wetlands Inventory Project. *Vegetatio* 118 (1–2), 153–169. <http://dx.doi.org/10.1007/BF00045197>.
- Winter, T.C., Rosenberry, D.O., 1995. The interactions of ground water with prairie pothole wetlands in the Cottonwood Lake area, east-central North Dakota, 1979–1990. *Wetlands* 15 (3), 193–211.
- Winter, T.C., Rosenberry, D.O., 1998. Hydrology of prairie pothole wetlands during drought and deluge: A 17-year study of the Cottonwood Lake wetland complex in North Dakota in the perspective of longer term measured and proxy hydrological records. *Clim. Chang.* <http://dx.doi.org/10.1023/A:1005448416571>.
- Wright, C., Gallant, A., 2007. Improved wetland remote sensing in Yellowstone National Park using classification trees to combine TM imagery and ancillary environmental data. *Remote Sensing Environ.* 107 (4), 582–605. <http://dx.doi.org/10.1016/j.rse.2006.10.019>.
- Wright, C.K., 2010. Spatiotemporal dynamics of prairie wetland networks: power-law scaling and implications for conservation planning. *Ecology* 91 (7), 1924–1930.
- Wright, C.K., Wimberly, M.C., 2013. Recent land use change in the Western Corn Belt threatens grasslands and wetlands. *Proc. Nat. Acad. Sci. U.S.A.* 110 (10), 4134–4139. <http://dx.doi.org/10.1073/pnas.1215404110>.
- Zedler, J.B., Kercher, S., 2005. Wetland resources: Status, trends, ecosystem services, and restorability. *Annu. Rev. Environ. Resour.* 30, 39–74. <http://dx.doi.org/10.1146/annurev.energy.30.050504.144248>.
- Zhu, L., Tateishi, R., 2006. Fusion of multisensor multitemporal satellite data for land cover mapping. *Int. J. Remote Sens.* 27 (5), 903–918. <http://dx.doi.org/10.1080/0143116031000139818>.
- Zhu, Z., Wang, S., Woodcock, C.E., 2015. Improvement and expansion of the Fmask algorithm: cloud, cloud shadow, and snow detection for Landsats 4–7, 8, and Sentinel 2 images. *Remote Sens. Environ.* 159, 269–277. <http://dx.doi.org/10.1016/j.rse.2014.12.014>.
- Zhu, Z., Woodcock, C.E., 2012. Object-based cloud and cloud shadow detection in Landsat imagery. *Remote Sens. Environ.* 118, 83–94. <http://dx.doi.org/10.1016/j.rse.2011.10.028>.